Driving the Photochemical Reaction Cycle of Proteorhodopsin and Bacteriorhodopsin Analogues by Photoisomerization of Azo Chromophores

(アゾベンゼンクロモフォアによるプロテオロドプシンとバクテリオロドプシンアナログのフォトサイクルの駆動)

A Thesis

Submitted for the Degree of

Doctor of Life Science

By

Shariful Haque

Laboratory of Smart Molecules

Transdisciplinary Life Science Course

Graduate School of Life Science

Hokkaido University, Japan

December, 2020

Declaration

I hereby declare that the matter embodied in this thesis entitled “Driving the Photochemical Reaction Cycle of Proteorhodopsin and Bacteriorhodopsin Analogues by Photoisomerization of Azo Chromophores” is the result of investigations carried out by me under the supervision of ***Prof. Nobuyuki Tamaoki*** at the Laboratory of Smart Molecules, Transdisciplinary Life Science Course, Graduate School of Life Science, Hokkaido University, Japan and it has not been submitted elsewhere for the award of any degree or diploma.

In keeping with the general practice of reporting scientific observations, due acknowledgement has been made whenever the work described has been based on the findings of the other investigators. Any omission that might have occurred by oversight or error of judgments is regretted.

Shariful Haque

Certificate

I hereby certify that the work described in this thesis entitle “Driving the Photochemical Reaction Cycle of Proteorhodopsin and Bacteriorhodopsin Analogues by Photoisomerization of Azo Chromophores” has been carried out by ***Shariful Haque***, under my supervision at the Laboratory of Smart Molecules, Transdisciplinary Life Science Course, Graduate School of Life Science, Hokkaido University, Japan.

Prof. Nobuyuki Tamaoki

(Research Supervisor)

Table of contents

1. Introduction

Retinal is a natural polyene chromophore that forms a highly efficient molecular energy transducer, rhodopsin, upon binding with the lysine residue in G helix of the protein opsin through a protonated Schiff base linkage.[1] Photoisomerization of the retinal unit in rhodopsin catalyzes a series of photophysical and photochemical phenomena that results in the conversion of light to electrical signals in animals and to chemical energy or electrical signals in microorganisms.[2] Furthermore, in microorganisms, rhodopsins bearing retinal in the all-*trans* configuration can act as molecular pumps, channels, and sensors.[3] Proteorhodopsin (PR) and bacteriorhodopsin (BR) are well studied microbial rhodopsins that have essentially the same structures and functions.[4,5] Photoexcitation of the retinal unit in PR or BR triggers a photocyclic reaction that drives the translocation of a proton across the membrane from the cytoplasmic (CP) side to the extracellular (EC) side, leading to a proton gradient that is coupled to adenosine triphosphate (ATP) synthesis.[6]

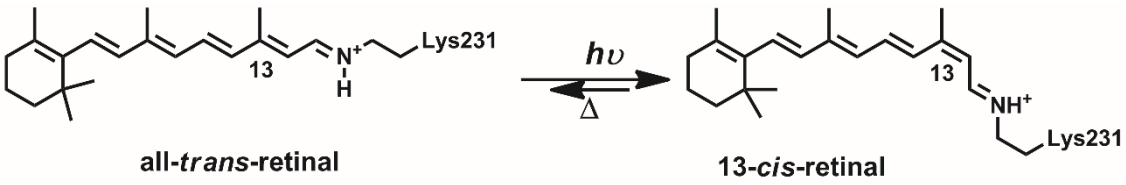

Fig. 1.1 Reversible photoreaction of retinal, bound with Lys231 residue of PR.

Azobenzene (azo), which undergoes reversible photoisomerization at its N=N double bond (Fig. 1.2), is a commonly used synthetic chromophore because of its high chemical stability, photofatigue resistance, and photosensitivity; its ready diversification; its strong UV–Vis–near-IR absorption band, which can be

modified through ring substitution;[7] and its readily induced and reversible photoisomerization.[8] Furthermore, because of its high compatibility with biopolymers, especially proteins, azobenzene has been used to impart enzymes,[9] ion channels,[10] and motor proteins[11] with photoswitching functions. Taking advantage of the photochromic properties of azo chromophores, the author suspected that azo derivatives could function an alternative to retinal and, thereby, modulate the photochromic properties of microbial rhodopsin and potentially lead to the development of artificial molecular machines. Moreover, unlike retinal, the molecular structure of an azo chromophore is readily modified, such that its photochromic properties could be tailored to modulate the photofunctional properties of microbial rhodopsin. The author is aware of only one previous attempt to develop azo chromophore–bound bacterioopsin derivatives, prepared from the azo chromophores (Fig. 1.3) 4-[[4′-(*N*,*N*-dimethylamino)phenyl-1′]azo]benzaldehyde (Az I) and 3-[4-[[4′-(*N*,*N*-dimethylamino)phenyl-1′]azo]phenyl-1]prop-2-enal (Az II).[12] Nevertheless, the photochemical reactions and photoinduced proton pumping functions of those azo analogues of BR were ambiguous.

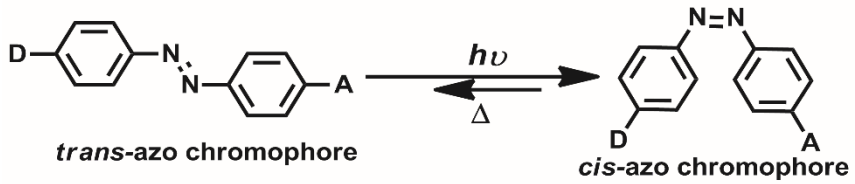

Fig. 1.2 Reversible photoreaction of push-pull type azobenzene. Where A and D are electron acceptor and donor groups respectively.

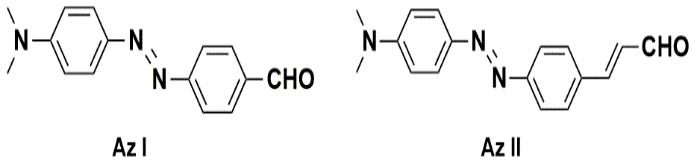

Fig. 1.3 Molecular structures of azo chromophores Az I and Az II.

In this dissertation, the author reports the development and characterization of azo chromophore Az I– and Az II–bound PR analogues (denoted PAz I and PAz II, respectively) and BR analogues (denoted BAz I and BAz II, respectively), as well as their photoinduced proton transfer reactions and photocycles. Moreover, the author also designed and synthesized a new push-pull type azo chromophore 4-[[2′,6′-dimethoxy, 4′-(N,N-dimethylamino)phenyl-1′]azo]-benzaldehyde denoted as Az III (Fig. 2.16A). It was found that Az III bound bacteriorhodopsin analogue denoted as BAz III showed the significantly higher photoinduced proton transfer reaction compared to BAz I and BAz II. Interestingly, the azo analogues of PR and BR did not exhibit proton pumping functions. Through analyses of azo analogues of PR mutant proteins, It was determined that the proton pumping malfunction of the azo analogues of PR and BR was the result of failures to evoke proton transfer reactions through the CP channels, even though these reactions could be induced through the EC channels. The author proposes herein a putative model for the proton transfer reaction mechanism of the azo analogues of PR and BR, based on our experimental data and those from other reports.

2. Results and Discussion

2.1 Formation of azo-POP complexes

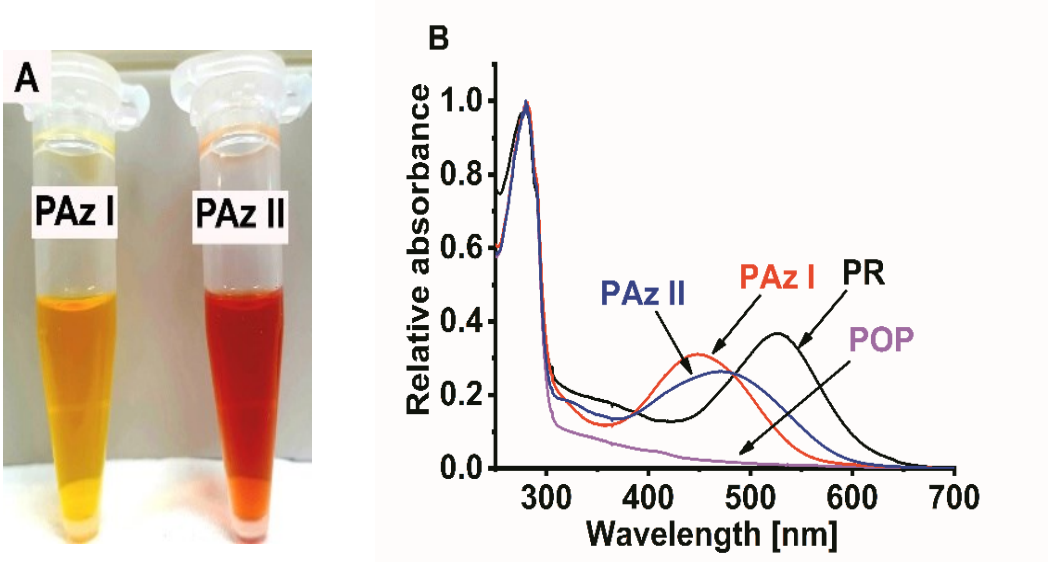

Fig. 2.1 Formation of azo-POP complexes PAz I and PAz II. **A.** Photograph of purified PAz I and PAz II pigments. **B.** UV-vis absorption spectra of POP (magenta line), PAz I (red line), PAz II (blue line), and wild-type PR (black line) in buffer (pH 7).

The author used UV–Vis absorption spectroscopy to confirm the formation of complexes between the azo chromophores and the proteoopsin protein (POP). The purified complexes PAz I and PAz II had characteristic yellow and deep-orange pigmentation, respectively (Fig. 2.1A). The purified POP protein (without dye-modification) conferred only an aromatic absorption band at 280 nm (Fig. 2.1B). In the case of wild-type PR, the interaction of retinal with POP caused a bathochromic shift of the absorption band of retinal from 380 to 520 nm (Fig. 2.1B), the result of forming a protonated Schiff base with the Lys231 residue.[5] Interestingly, both PAz I and PAz II exhibited characteristic absorption bands in

the visible region (Fig. 2.1B). The interactions of the azo chromophores with POP also caused bathochromic shifts of the absorption bands of the chromophores: for Az I, from 412 to 448 nm in PAz I; for Az II, from 387 to 472 nm in PAz II (Table 2.1). It has been reported previously that forming *n*-butyl Schiff bases from the azo chromophores Az I and Az II in MeOH leads to red-shifting of their absorption bands to 436 and 446 nm, respectively; furthermore, subsequent protonation of these *n*-butyl Schiff bases in MeOH causes further red-shifts of the absorption bands to 465 and 504 nm, respectively.[12] Therefore, the author presumes that the red-shifts of the absorption bands of PAz I and PAz II were a consequence of the formation of Schiff bases between the azo chromophores and the Lys231 residue of POP. Nevertheless, the blue-shifts of the absorption bands of PAz I and PAz II relative to those of the protonated *n*-butyl Schiff bases of the azo chromophores Az I and Az II might indicate that the Schiff bases of PAz I and PAz II were not protonated in the dark state. These artificial pigments PAz I and PAz II appear to be very stable, with no changes in color or spectral properties observed after long-term storage at 4 °C.

Az I and Az II are push/pull–type azo chromophores that exist in the *trans* conformation in the dark state. Upon illumination, they isomerize to the *cis* form, and then return thermally to the *trans* form. Thus, their photochemical reactions are similar to those of retinal unit within microbial rhodopsins. Nevertheless, as mentioned above, their Schiff bases should be non-protonated in the unphotolized state. Thus, the Az I and Az II units cannot drive the proton transfer reactions observed in natural proton pump rhodopsins, in which the protonated Schiff base initially donates a proton to the neighboring Asp residue (Asp97 for PR; Asp85 for BR). For azo-rhodopsin analogues, however, the *trans*-to-*cis*

isomerization would increase the basicity of the Schiff base. Thus, the Az I and Az II units might drive the “opposite” proton transfer reaction, in which the Schiff base first accepts a proton from a dissociable residue or water molecule. The isomerizations of the Az I and Az II units would presumably induce substantial protein conformational changes, similar to those induced by the retinal unit. Thus, the author expected deprotonations of the dissociable residues in the CP channels (i.e., Glu108 for PR; Asp96 for BR) and resultant proton donations to the Schiff bases. If these kinds of reactions would evoke subsequent proton transfers, the author might observe proton release/uptake reactions on the EC and CP sides and also proton pump activity across the membrane.

Table 2.1 UV-vis absorption maxima (λ_{max}) of azo chromophores and azo analogues of PR and BR in buffer at pH 7.

Chromophore	**λ_{max} (nm) of chromophore**	**λ_{max} (nm) of chromophore–POP complex**	**λ_{max} (nm) chromophore–BOP complex**
Az I	412	448	458
Az II	387	472	462
Az III	464	485	483
Retinal	380	520	570

2.2 Photoinduced proton transfer of PAz I and PAz II

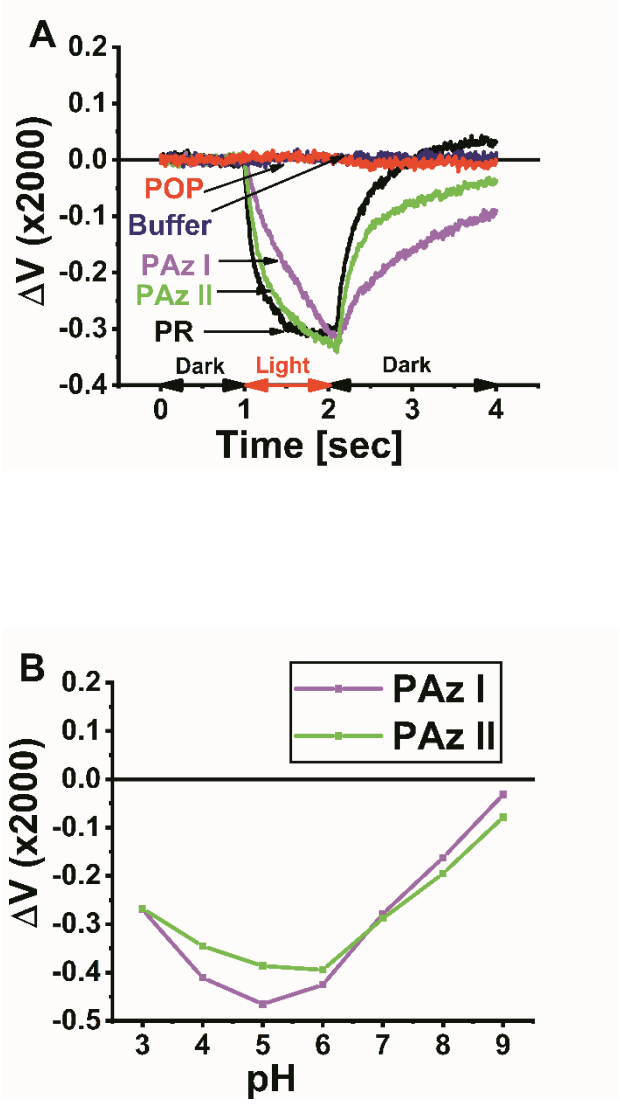

Fig. 2.2 Photoinduced proton transfer of azo analogues of PR. **A.** Changes in the photoinduced proton transfer potentials of PAz I (magenta), PAz II (green), wild-type PR (black), POP (red), and buffer (navy) at pH 7. **B.** pH-Dependent changes in the photoinduced proton transfer potentials of PAz I (magenta) and PAz II (green).

The author examined the photoinduced proton uptake and release capabilities of PAz I and PAz II by studying their proton transfer reactions in a photoelectrochemical cell featuring a transparent indium tin oxide (ITO) electrode that was highly pH-sensitive, such that it could monitor time-dependent changes in pH of the medium at any pH.[13,14] This photoelectrochemical cell has been used previously to examine the photoinduced proton transfer reactions of BR and PR.[15–17] As a positive control sample, the author used wild-type PR; it provided a light-induced potential signal (Fig. 2.2A) similar to that reported previously.[15] Upon absorption of light, wild-type PR undergoes the following proton transfer sequence: transfer of the proton from the protonated Schiff base to Asp97, uptake of the proton from the CP side via the Glu108 residue, and release of the proton from the Asp97 residue to the EC side.[18–20] Thus, the observed downward and upward deflections of the ITO potential signal of the wild-type PR represent a local decrease and increase, respectively, in pH. Interestingly, both PAz I and PAz II provided photoinduced potential signals (Fig. 2.2A), indicating that they underwent photoinduced proton transfer reactions. Moreover, like wild-type PR, PAz I and PAz II also experienced initial proton uptake followed by proton release. Fig. 2.3 displays the photoinduced conformational changes and proton transfer reactions of PAz I and PAz II. Upon illumination, the *cis* isomers of PAz I and PA z II were formed, causing the basicity of their Schiff bases to increase, resulting in the uptake of a proton. Subsequent thermal isomerization led to formation of the protonated transient *trans* isomers of PAz I and PAz II, thereby decreasing the basicity of the Schiff bases and causing the release of the proton, followed by recovery of the initial state.

To confirm the mechanism behind the voltage changes upon photoirradiation, the author recorded the pH-dependent voltage changes of PR analogues at values of pH between 3 and 9. Fig. 2.2B plots the maximum changes in the photoinduced potentials of PAz I and PAz II with respect to the pH. Both PAz I and PAz II exhibited higher proton transfer activities in the pH range from 4 to 6. As mentioned above, it is likely that, in the dark state, PAz I and PAz II featured their azo chromophore units in the more stable *trans* form, bound (most probably) through a non-protonated Schiff base. At values of pH of less than 3, the Schiff bases of PAz I and PAz II would already be protonated in the *trans* state and, thus, their isomerizations would not drive the proton transfer reactions. On the other hand, at values of pH higher than 7, the Schiff bases cannot capture protons, even in their *cis* states, because the pH is higher than their values of pK_a. Thus, there is a suitable pH range in which a proton can be transferred upon photoisomerization from the *trans* to *cis* state with a change in pK_a.

The author performed several control experiments to confirm the light-induced potential signals of PAz I and PAz II. As a negative control, the bare ITO electrode (buffer), upon illumination with continuous Xe light, did not evoke a change in the voltage signal (Fig. 2.2A). In other words, continuous irradiation with Xe light did not affect the ITO electrode. Furthermore, the author tested the photoinduced proton transfer of the azo chromophores themselves after incorporation in Egg-phosphatidylcholine (Egg-PC) lipid membrane, using the same photoelectrochemical cell at various values of pH between 3 and 9. The author observed no photoinduced potential signals for either lipid-incorporated

azo chromophore. Thus, neither the azo (-N=N-) nor dimethylamine [$(CH_3)_2N$-] groups of the azo chromophores Az I and Az II accepted or released a proton upon illumination. In addition, Egg-PC–incorporated POP did not present any change in the photoinduced potential signal (Fig. 2.2A), confirming that the observed signals of PAz I and PAz II were not artifacts.

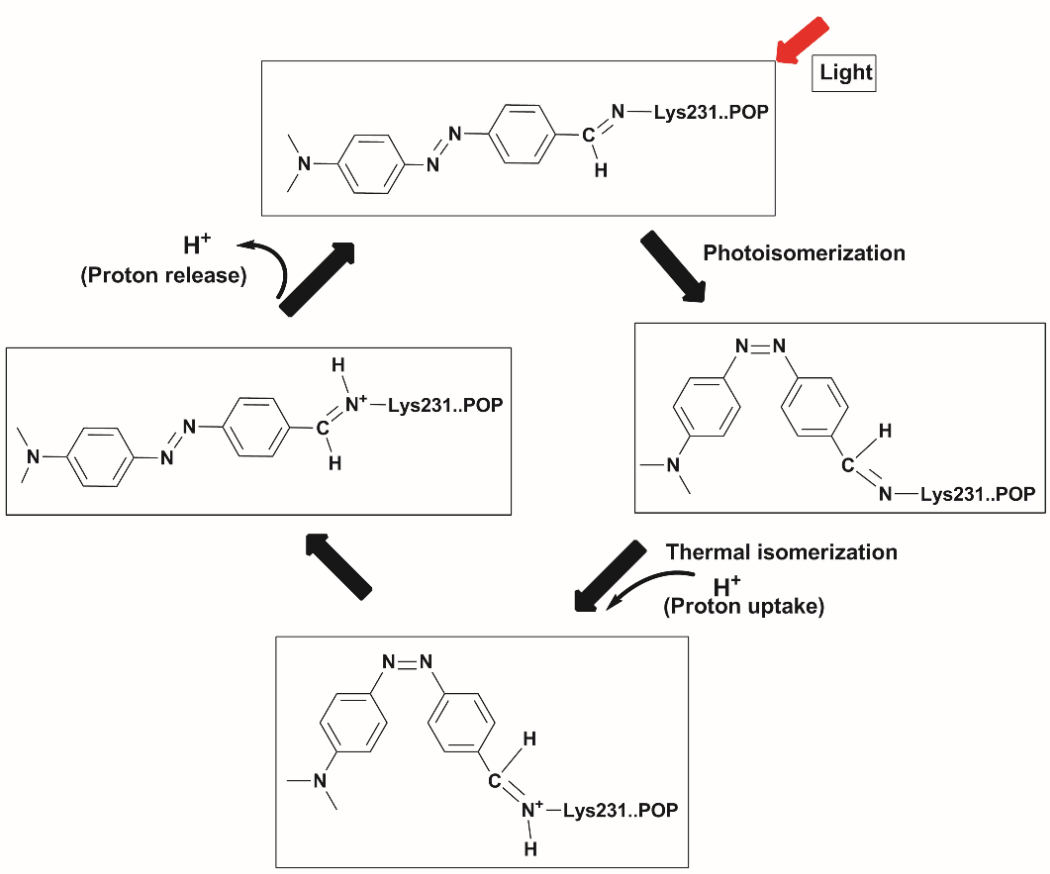

Fig. 2.3 Putative model of proton transfer reaction of PAz I.

2.3 Photoinduced proton pumping of PAz I and PAz II

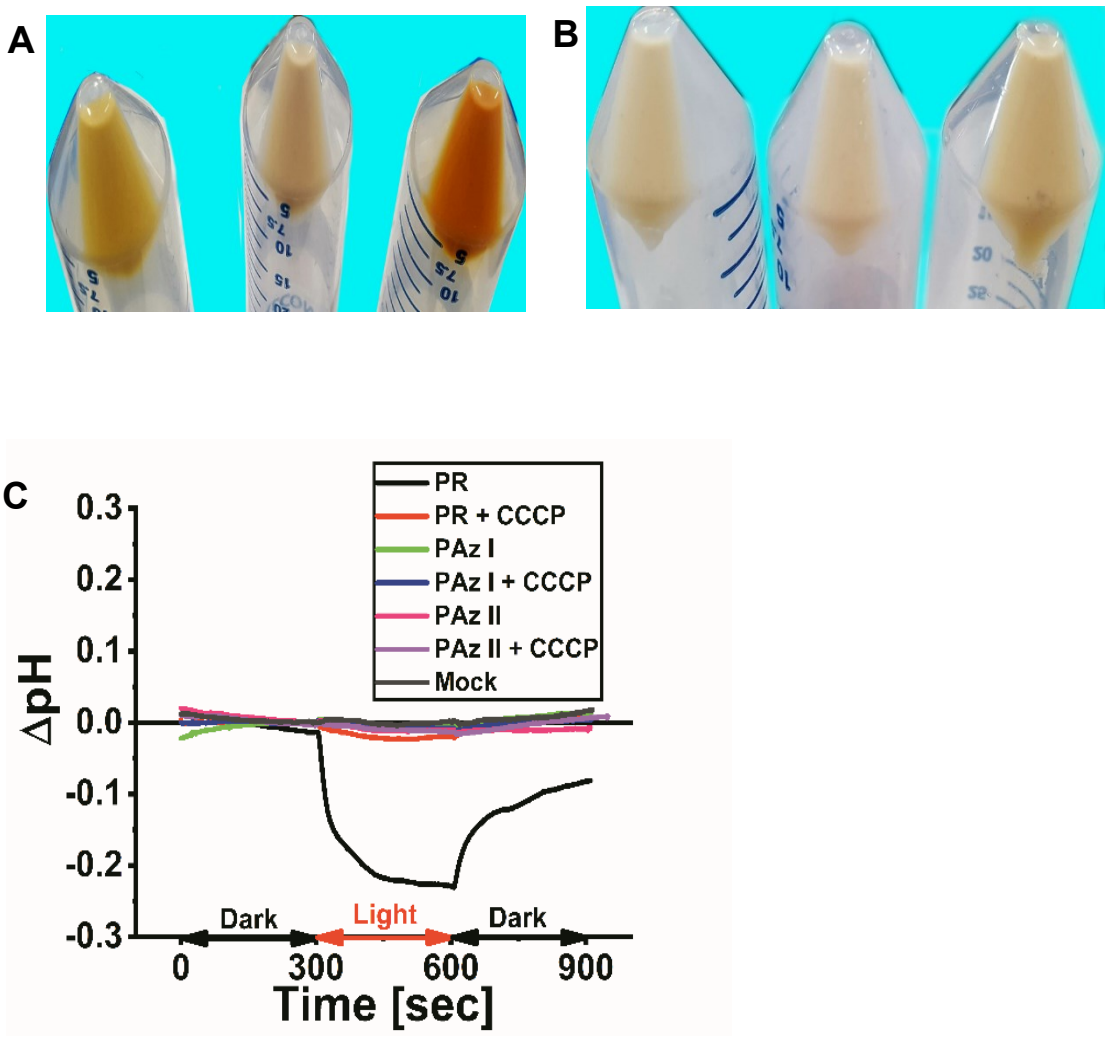

Fig. 2.4 Light-driven proton pumping activity of PAz I and PAz II. **A.** Photographs of PO-expressed *E. coli* cells solids incubated with azo chromophore Az I (Left) and Az II (Right) and without azo chromophore (Middle). **B.** Photograph of PO-unexpressed *E. coli* cells solids incubated with azo chromophores Az I (Left) and Az II (Right) and without azo chromophore (Middle). **C.** Light-driven changes in pH of wild-type PR– and PAz I– and PAz II–expressing *E. coli* cell suspensions, in the presence and absence of CCCP.

To determine the proton pumping functions of the azo analogues of PR, the author expressed PAz I and PAz II in *Escherichia coli* cells, which acquired yellow and deep-orange pigmentation, respectively (Fig. 2.4A). As expected, POP-unexpressed *E. coli* cells incubated with these azo chromophores did not have such colors (Fig. 2.4B). The pigmentation of these *E. coli* cells indicates that specific interactions existed between the azo chromophores and POP. The author used flash photolysis to confirm the expression of PAz I and PAz II in the *E. coli* cells. The sonicated *E. coli* cells expressing PAz I and PAz II experienced flash-induced changes in their transient absorbances at characteristic values of λ_{max} (not shown here). As a positive control, the wild-type PR provided a negative change in pH upon illumination (Fig. 2.4C); this change was inhibited significantly upon the addition of carbonyl cyanide *m*-chlorophenylhydrazone (CCCP), indicative of photoinduced proton pumping.[5] On the other hand, PAz I and PAz II provided no changes in pH upon illumination, regardless of whether CCCP was present (Fig. 2.4C). These data indicate that PAz I and PAz II cannot pump protons across the membrane upon illumination.

2.4 Photochemical reaction of PAz I and PAz II

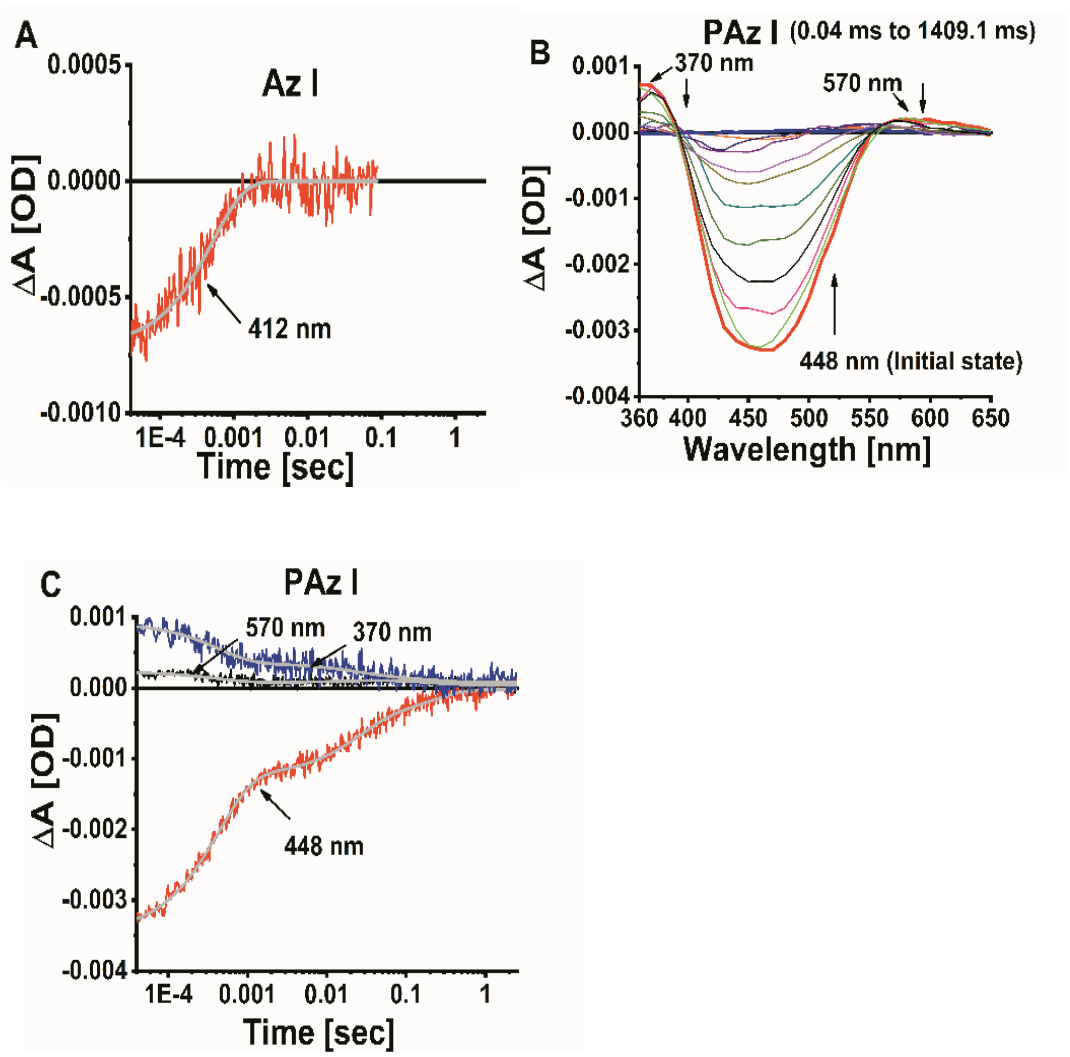

Fig. 2.5 Flash photolysis of Az I and PAz I. **A.** Experimental (red) and simulated (light gray) flash photolysis curves of Az I at λ_{max}. **B.** Flash-induced light-minus-dark difference absorption spectra of PAz I over the spectral range 360–650 nm and the time range of 0.04–1409.10 ms. Red and blue lines represent the spectra recorded at 0.04 and 1409.10 ms, respectively. The directions of evolution of the spectral changes are indicated by arrows. **C.** Experimental and simulated flash photolysis curves of PAz I recorded at three characteristic wavelengths. Fitting curves are provided as light gray lines.

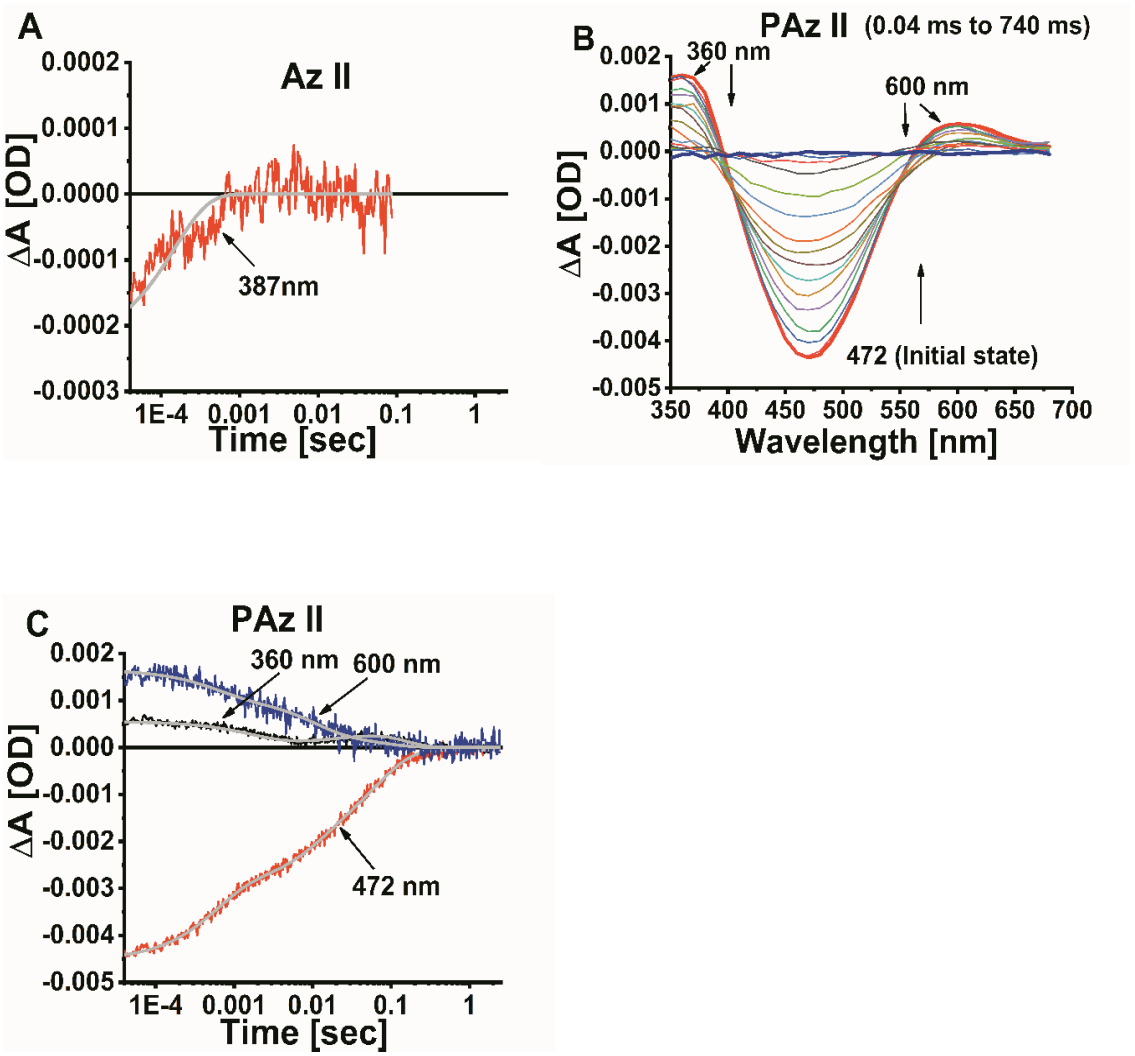

Fig. 2.6 Flash photolysis of Az II and PAz II. **A.** Experimental (red) and simulated (light gray) flash photolysis curves at λ_{max} of Az II. **B.** Flash-induced light-minus-dark difference absorption spectra of PAz II over the spectral range 350–700 nm and the time range of 0.04–740.0 ms. Red and blue lines represent the spectra recorded at 0.04 and 740.0 ms, respectively. The directions of evolution of the spectral changes are indicated by arrows. **C.** Experimental and simulated flash photolysis curves of PAz II recorded at three characteristic wavelengths. Fitting curves are provided as light gray lines.

Upon absorption of visible light, photoexcitation of the retinal unit in microbial rhodopsin induces the photochemical reaction and conformational changes of the protein, driving the sequential generation of various photo-intermediates, followed by a return to the unphotolyzed form of the protein. During this linear cyclic series of photochemical reactions (the so-called photocycle), cognate biological functions of microbial rhodopsin are accomplished. To determine whether PAz I and PAz II could undergo cyclic photoreactions similar to retinal microbial rhodopsin upon illumination, the author used flash photolysis to study the photochemical reactions of both the azo chromophores and the azo-POP complexes. The azo chromophores Az I and Az II are push/pull–type azobenzenes whose rates of thermal isomerization depend strongly on the polarity of the solvent.[21] The author used the same buffer solution at pH 7 to study the photoreaction kinetics of the azo chromophores and their POP complexes. To avoid large scattering artifacts arising from the laser flash, plots were recorded after 40 μs. The azo chromophores Az I and Az II underwent flash-induced changes in their transient absorbances and very fast thermal recoveries at characteristic values of λ_{max} (Fig. 2.5A for Az I; Fig. 2.6A for Az II), indicating reversible photoinduced photoisomerization of the azo chromophores. The flash photolysis curves of Az I and Az II were fitted well by single-exponential forms of first-order rate equations [$y = m_1 * \exp(-t/m_2)$, where t is the time (s) and m_1 and m_2 are fitting parameters]. The residual sums of squares (RSS) from fitting of the flash photolysis curves of Az I and Az II were 2.03×10^{-6} and 3.42×10^{-6}, respectively. The thermal decay rate constant and lifetime of the *cis* isomer, obtained from fitting the flash photolysis curves, were 1.94×10^{3} s^{-1} and

0.51 ms, respectively, for Az I and 6.77×10^3 s^{-1} and 0.15 ms, respectively, for Az II.

Fig. 2.5B and Fig. 2.6B present the flash-induced light-minus-dark absorption spectra of PAz I and PAz II, respectively. Upon excitation of the original state, a negative peak appeared near the absorption maximum at 448 nm for PAz I and at 472 nm for PAz II within 40 μs; it gradually recovered within 1409.10 ms for PAz I and 740.0 ms for PAz II, indicating the depression and recovery of their original states. Simultaneously, positive absorption bands appeared near 370 and 570 nm for PAz I and near 360 and 600 nm for PAz II, gradually decaying over time. These features indicate the cyclic photoreactions of PAz I and PAz II. Moreover, the slower photoreactions of PAz I and PAz II, relative to those of their isolated azo chromophores, are consistent with the interactions of the azo chromophore with the protein POP. Fig. 2.5C and Fig. 2.6C display the flash-induced time-dependent absorbance changes at selective wavelengths of 370, 448, and 570 nm for PAz I and 360, 472, and 600 nm for PAz II, respectively. To obtain the photoreaction kinetics of PAz I and PAz II, the author fits their flash photolysis curves using the following sequential reaction model

$$\mathrm{P_0} \xrightarrow{h\nu} \mathrm{P_1} \xrightarrow{k_1} \mathrm{P_2} \xrightarrow{k_2} \mathrm{P_3} \xrightarrow{k_3} \mathrm{P_0}$$

where P_0 and P_1–P_3 represent their initial states and first, second, and third kinetically defined photointermediates, respectively, and k_1–k_3 are the thermal decay rate constants of the three successive steps. The flash-induced absorbance changes Y (λ,t) as a function of time were fitted to equation

$$Y(\lambda, t) = \epsilon P_1(\lambda)[P_1(t)] + \epsilon P_2(\lambda)[P_2(t)] + \epsilon P_3(\lambda)[P_3(t)] + \epsilon P_0(\lambda)[P_0(t)] \ldots . (1)$$

where the parameters ϵ are the unknown molar absorptivities of the species at the specified wavelengths. The species concentrations were obtained using the following expressions, by solving the coupled equations for a four-step consecutive first-order reaction:[22]

$$P_1(t) = P_1^0 e^{-k_1 t} \ldots . (2)$$

$$P_2(t) = \frac{k_1 P_1^0}{k_2 - k_1} (e^{-k_1 t} - e^{-k_2 t}) \ldots . (3)$$

$$P_3(t) = P_1^0 [\frac{k_1 k_2}{(k_3 - k_1)(k_2 - k_1)} e^{-k_1 t} - \frac{k_1 k_2}{(k_3 - k_2)(k_2 - k_1)} e^{-k_2 t} + \frac{k_1 k_2}{(k_3 - k_2)(k_3 - k_1)} e^{-k_3 t}] \ldots . (4)$$

$$P_0(t) = P_1^0 [1 - \frac{k_2 k_3}{(k_2 - k_1)(k_3 - k_1)} e^{-k_1 t} - \frac{k_1 k_3}{(k_1 - k_2)(k_3 - k_2)} e^{-k_2 t} - \frac{k_1 k_2}{(k_1 - k_3)(k_2 - k_3)} e^{-k_3 t}] \ldots . (5)$$

where, P_1^0 is the initial molar concentration of transient intermediate P_1, determined from the flash-induced change in absorbance at initial time point of fitting and the experimental value of molar absorptivity of P_0 at λ_{max}. The flash-photolysis curve at λ_{max} was fitted by adding the change in absorbance at initial time point of fitting to equation (1). The flash photolysis curves at other wavelengths were fitted using derived decay rate constants for the three steps.

The flash photolysis curves of PAz I and PAz II were fitted well by these equations [fitting curves are provided in light gray in Fig. 2.5C for PAz I and in Fig. 2.6C for PAz II]. For example, the RSS values from the fitting of the data for PAz I at 370, 448, and 570 nm were 3.42×10^{-6}, 5.43×10^{-6}, and 9.33×10^{-6}, respectively (Table 2.2).

Fig. 2.7 summarizes the photoreaction kinetics of PAz I as a typical example. The thermal decay rate constants of the three transient steps were 2.34×10^{3}, 42.39, and 4.97 s^{-1}, respectively (Table 2.2). During the photoreaction, the molar absorptivities of the three transient species of PAz I changed at the various wavelengths (Table 2.2). Upon formation of intermediate P_1, the molar absorptivity increased significantly at 370 nm (ϵP_1 6.85×10^{3} M^{-1} cm^{-1}) and moderately at 570 nm (ϵP_1 1.71×10^{3} M^{-1} cm^{-1}), but decreased sharply at the value of λ_{max} of ϵP_1 448 nm (286.7 M^{-1} cm^{-1}), relative to those of the initial state P_0. These phenomena suggest that upon the formation of P_1, the π→π* absorption band of the chromophore shifted to shorter wavelength and the n→π* electronic transition (near 570 nm) was allowed, resulting in an increase in intensity; furthermore, they suggest that the intermediate P_1 was the *cis* isomer of the initial state. Upon formation of the intermediate P_2, the molar absorptivity of PAz I increased significantly at 448 nm (ϵ 1.69×10^{4} M^{-1} cm^{-1}) but decreased at other two wavelengths of 370 nm (2.60×10^{3} M^{-1} cm^{-1}) and 570 nm (898.7 M^{-1} cm^{-1}), relative to those of intermediate P_1, possibly indicating that the π→π* absorption band had shifted to longer wavelength (near 448 nm). The red-shifting of the π→π* absorption band may support the photoinduced proton uptake reaction of PAz I. Compared with the molar absorptivity of P_0 at 448 nm, the significantly lower molar absorptivity of P_2 at 448 nm might indicate that P_2 is also

another transient *cis* isomer of the initial state. The intermediate P_2 decayed thermally with a rate constant of 42.39 s^{-1} to form the intermediate P_3. Upon formation of P_3, the molar absorptivity of PAz I increased further at 448 nm (ϵ 2.30 × 10^4 M^{-1} cm^{-1}), but it decreased at 370 nm (1.24 × 10^3 M^{-1} cm^{-1}) and 570 nm (567.6 M^{-1} cm^{-1}), relative to those of P_2. The molar absorptivities of intermediate P_3 at the various wavelengths were close to those of the initial state P_0, suggesting that P_3 is a transient *trans* isomer of the initial state. Finally, the intermediate P_3 decayed thermally to the initial state with a rate constant of 4.97 s^{-1}. For PAz I, the simulated molar absorptivities of the initial state P_0 were 2.59 × 10^4 M^{-1} cm^{-1} at 448 nm, ϵP_0 588.2 M^{-1} cm^{-1} at 370 nm, and 319.2 M^{-1} cm^{-1} at 570 nm; these values are reasonably close to the experimental values of 2.54 × 10^4, 530.0, and 340.0 M^{-1} cm^{-1}, respectively. The author observed similar photoreaction kinetics in the case of PAz II; Table 2.3 provides the results of fitting the data obtained at wavelengths of 360, 472, and 600 nm. Thus, our kinetics analyses of the photoreactions of PAz I and PAz II confirmed that the thermal decay processes of their azo chromophores units were dissimilar to the single-exponential processes that the author determined for the isolated azo chromophores. Our data strongly suggest that, upon illumination, PAz I and PAz II undergo cyclic photoreactions featuring three transient species.

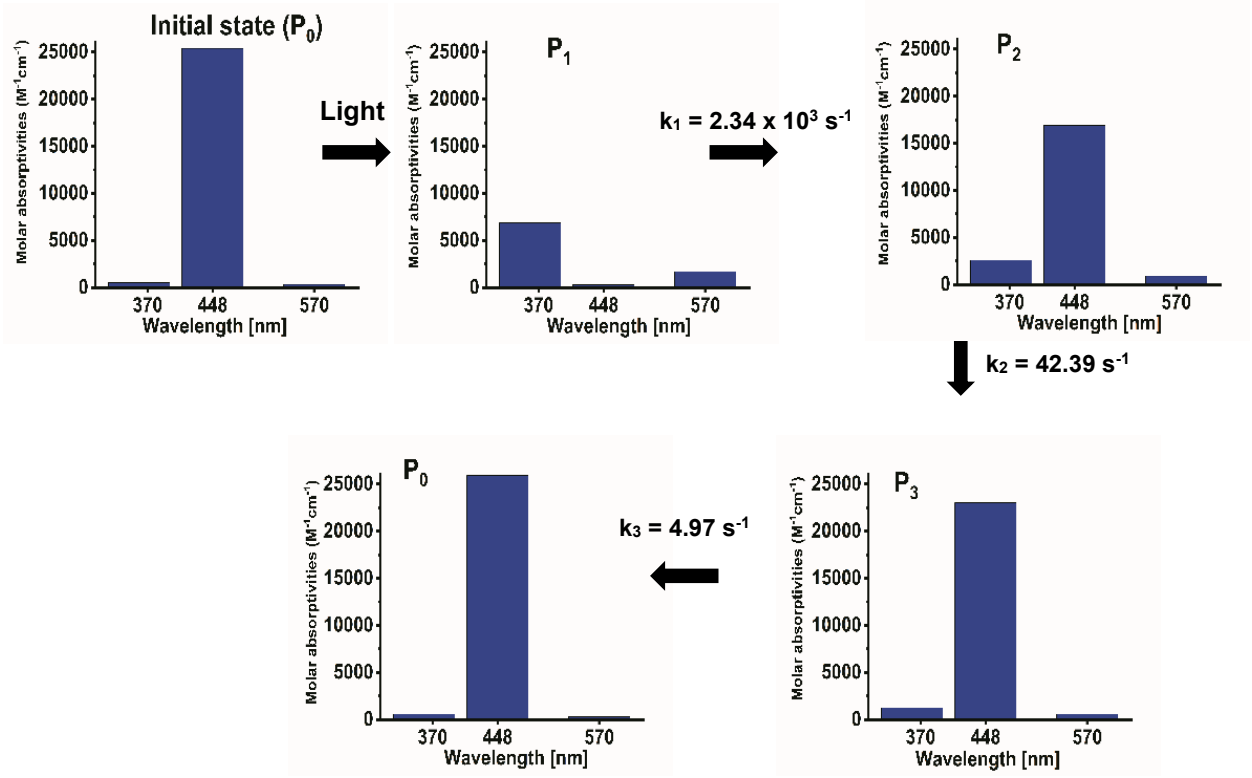

Fig. 2.7 As a typical example, schematic presentation of formation of different transient intermediates along with their molar absorptivity changes at different wavelength during photoreaction of PAz I.

Table 2.2 Parameters from fitting of the flash photolysis data of PAz I at 448, 370, and 570 nm.

Wave-length (nm)	k_1 (s^{-1})	k_2 (s^{-1})	k_3(s^{-1})	ϵP_1 (M^{-1} cm^{-1})	ϵP_2 (M^{-1} cm^{-1})	ϵP_3 (M^{-1} cm^{-1})	ϵP_0 (M^{-1} cm^{-1})	RSS
448	$2.34 \times 10^3 \pm 45.0$	42.39 ± 4.0	4.97 ± 0.86	286.7 ± 78.0	$1.69 \times 10^4 \pm 101.0$	$2.30 \times 10^4 \pm 330.0$	$2.59 \times 10^4 \pm 84.00$	3.42×10^{-6}
370	2.34×10^3	42.39	4.97	$6.85 \times 10^3 \pm 113.0$	$2.60 \times 10^3 \pm 82.00$	$1.24 \times 10^3 \pm 122.0$	588.2 ± 85.00	5.43×10^{-6}
570	2.34×10^3	42.39	4.97	$1.71 \times 10^3 \pm 47.0$	898.7 ± 50.00	567.6 ± 34.18	319.2 ± 35.00	9.33×10^{-6}

Table 2.3 Parameters from fitting of the flash photolysis data of PAz II at 472, 360, and 600 nm.

Wave-length (nm)	k_1 (s^{-1})	k_2 (s^{-1})	k_3(s^{-1})	ϵP_1 (M^{-1} cm^{-1})	ϵP_2 (M^{-1} cm^{-1})	ϵP_3 (M^{-1} cm^{-1})	ϵP_0 (M^{-1} cm^{-1})	RSS
472	1.77×10^3 ± 62.22	102.0 ± 11.24	14.72 ± 0.59	130.8 ± 44.77	7.69×10^3 ± 120.0	1.33×10^4 ± 366.0	2.12×10^4 ± 36.0	3.12×10^{-6}
360	1.77×10^3	102.0	14.72	7.78×10^3 ± 93.0	4.88×10^3 ± 94.0	1.18×10^3 ± 115.0	14.40 ± 6.37	1.05×10^{-6}
600	1.77×10^3	102.0	14.72	2.96×10^3 ± 50.0	1.25×10^3 ± 51.0	991.0 ± 63.0	220.1 ± 32.0	3.04×10^{-6}

2.5 Mutational analysis of PAz I and PAz II

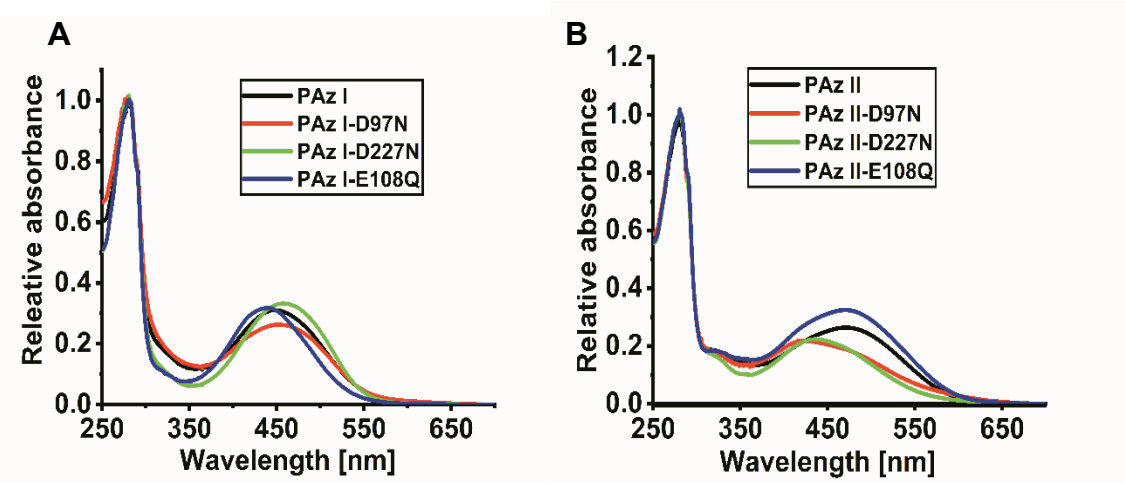

Fig. 2.8 A. UV-vis absorption spectra of PAz I (black), PAz I-D97N (red), PAz I-D227N (green) and PAz I-E108Q (blue). **B.** UV-vis absorption spectra of PAz II (blank), PAz II-D97N (red), PAz II-D227N (green) and PAz II-E108Q (blue).

The author performed mutational analyses to better understand the proton transfer reaction pathways of PAz I and PAz II and to confirm the importance of the protein POP. The author selected three key amino acid residues of POP and replaced them with neutral residues (D97N, D227N, E108Q). The author prepared the azo analogues of the three POP mutant proteins (denoted PAz I-D97N, PAz I-D227N, and PAz I-E108Q and PAz II-D97N, PAz II-D227N, and PAz II-E108Q) and investigated them using UV–Vis spectroscopy, flash photolysis, and studies of their photoinduced proton transfer. In wild-type PR, the D97 residue, located at the EC side, is the proton acceptor from the protonated Schiff base; the PR-D97N mutant almost completely blocks the formation of the M intermediate, having a deprotonated Schiff base, and inhibits the proton

transfer reaction.[18] On the other hand, the E108 residue of PR, located at the CP side, is the proton donor to the deprotonated Schiff base; the PR-E108Q mutant significantly retards the M decay and impairs the proton transfer reaction.[18,23] In PR, the D227 residue, a secondary counterion to the protonated Schiff base, controls the photoisomerization pathways toward 13-*cis* or 9-*cis* photoproducts;[24,25] the D227N mutation leads to the formation of a long-lived photoproduct with a deprotonated Schiff base.[26] The author recorded UV–Vis absorption spectra to characterize all three mutant analogues of PAz I and PAz II (Fig. 2.8A and Fig. 2.8B, respectively). The author observed spectral blue-shifts of 56 nm for PAz II-D97N and 35 nm for PAz II-D227N, in contrast to the small red-shifts of 8 nm for PAz I-D97N and 10 nm for PAz I-D227N. The mutant analogue PAz II-E108Q did not experience any shift of its spectral band at 472 nm, but PAz I-E108Q underwent a small blue-shift of its absorption band at 440 nm. These absences of spectral shifts probably reflect the electrostatic isolation between the Schiff base regions and the E108 side chains. The E108 residue is located in the middle of the hydrophobic CP channel and, thus, is protonated in the dark state. On the other hand, the small red-shifts observed for the D97N and D227N mutants may reflect that these Asp residues were originally protonated in the dark state, unlike to those in natural proton pumps.

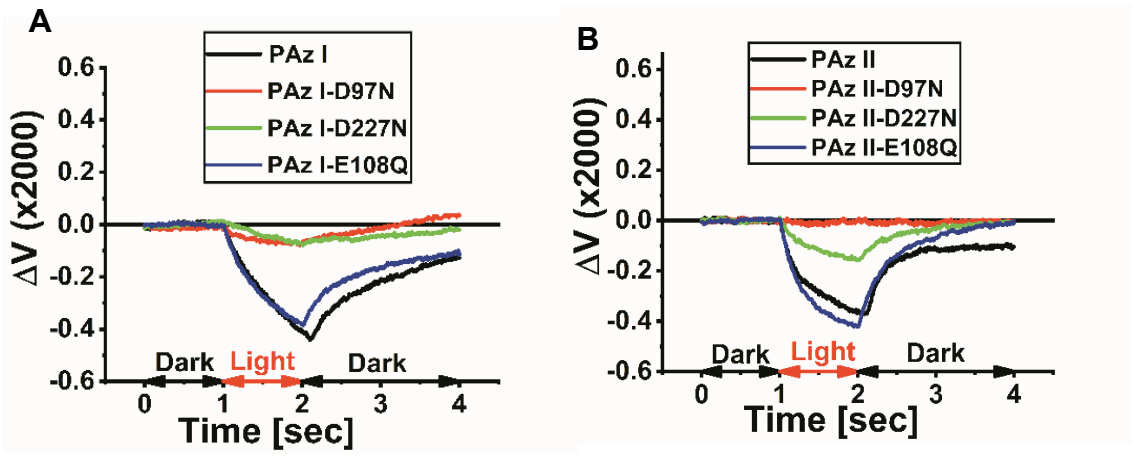

Fig. 2.9 A. Change in the signals for photoinduced proton transfer of PAz I (black), PAz I-D97N (red), PAz I-D227N (green), and PAz I-E108Q (blue). **B.** Change in the signals for photoinduced proton transfer of PAz II (blank), PAz II-D97N (red), PAz II-D227N (green) and PAz II-E108Q (blue).

The PAz I-E108Q and PAz II-E108Q mutant analogues did not experience any impairment of their photoinduced proton transfer reaction signals (Fig. 2.9A and 2.9B, respectively), indicating that E108 did not act as proton donor in either PAz I or PAz II. Moreover, PAz I-E108Q and PAz II-E108Q exhibited flashed-induced changes in their transient absorbance at three representative wavelengths (Fig. 2.10C and Fig. 2.11C respectively), identical to those of PAz I and PAz II, respectively, indicating that the E108 residue was not involved in the photoreaction cycles of PAz I and PAz II. These data also suggest that PAz I and PAz II did not take up the proton from the CP side. It has been established previously that the CP halves of both BR and PR undergo large scale conformational changes that are needed for the influx of bulk water in the later stages of their respective photocycles.[27] This influx of water allows the formation

of a stable water wire to bridge the gap of 10–15 Å that exists between the proton donor and the Schiff base and to transport the proton from E108 to the Schiff base.[28–31] Our data from the flash photolysis and proton transfer reactions of the E108Q mutant analogues of PAz I and PAz II suggest that CP opening and subsequent hydration did not occur in PAz I and PAz II.

The PAz I-D97N mutant underwent a significantly impaired photoinduced proton transfer reaction (Fig. 2.9A). It exhibited flash-induced depletion of its initial state and a subsequent slow recovery (Fig. 2.10A), even though such phenomena were not observed in the case of PAz II-D97N (Fig. 2.11A). Moreover, the PAz II-D97N mutant didn't experience the show proton transfer reaction (Fig. 2.9B). Because the Schiff bases of PAz I and PAz II were most probably not protonated in the dark state, the abolishment of the photoinduced proton transfers of the D97N mutant analogues of PAz I and PAz II suggests that the carboxylic acid residue D97 in PAz I and PAz II might have acted as the proton donor in the initial step of the photocycle. These data also suggest that the azo analogues of PAz I and PAz II accepted the proton from the EC side upon illumination. As mentioned above, the D97 residues should not have been protonated in the dark states. Thus, they became transiently protonated and then donated protons to the respective Schiff bases. Ultimately, these protons should have been released at the same side. The resultant proton circulations at the EC side would lead to no observation of proton pumping activity.

Meanwhile, the photoinduced potential signals of the D227N mutant analogues of PAz I and PAz II were significantly lower than those of PAz I and PAz II, respectively (Fig. 2.9A and Fig. 2.9B respectively), indicating significant impairment of the proton transfer reaction. Moreover, both PAz I-D227N and PAz

II-D227N underwent flash-induced depletion of their initial states with very slow thermal recoveries at λ_{max} (Fig. 2.10B and Fig. 2.11B, respectively), presumably causing the significant impairments of their proton transfer reactions. These data suggest that the D227 residues may have interacted with the Schiff bases to regulate the photoreactions of PAz I and PAz II.

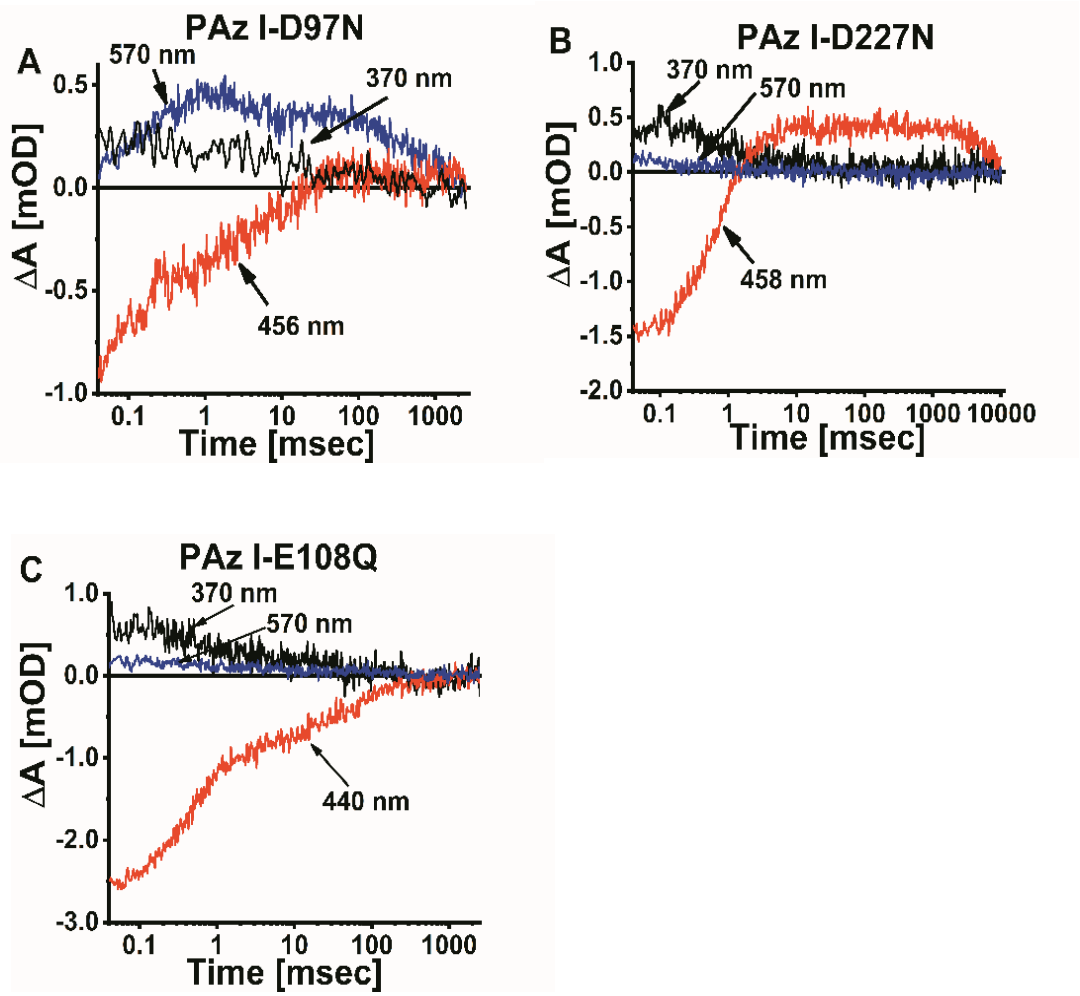

Fig. 2.10 Flash-induced absorbance changes at three characteristics wavelengths for **(A)** PAz I-D97N, **(B)** PAz I-D227N, and **(C)** PAz I-E108Q.

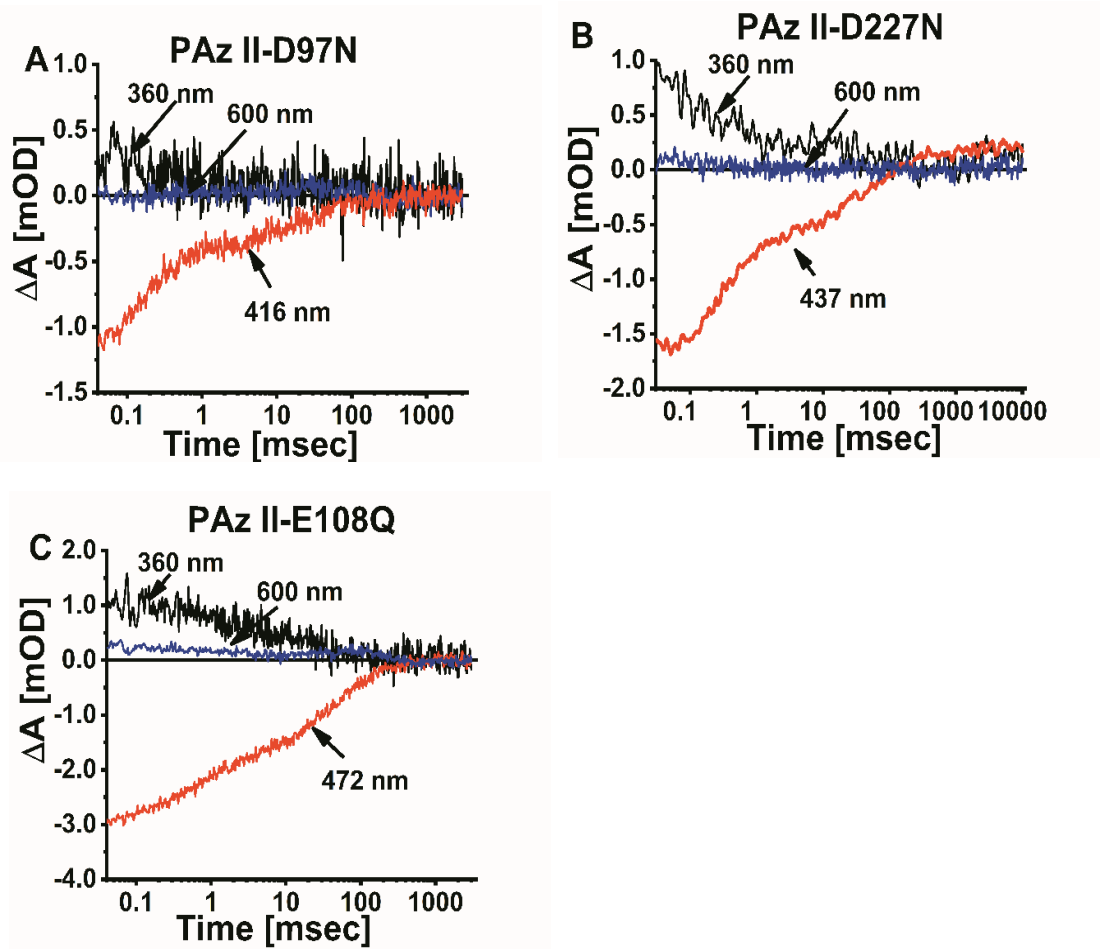

Fig. 2.11 Flash-induced absorbance changes at three characteristics wavelengths for **(A)** PAz II-D97N, **(B)** PAz II-D227N, and **(C)** PAz II-E108Q.

2.6 Formation of azo-bacterioopsin complexes BAz I and BAz II

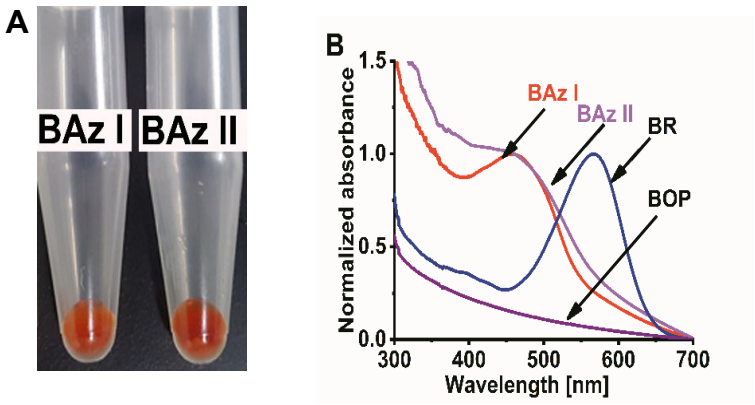

Fig. 2.12 Formation of BAz I and BAz II analogues. **A**. Photograph of purified-solid BAz I and BAz II. **B**. Normalized UV–Vis absorbance spectra of purified wild-type BR (navy), BOP (pink), BAz I (red), and BAz II (magenta).

Although the photoinduced pH changes of Az I and Az II chromophore–bound bacterioopsin have been reported previously,[12] it remained uncertain whether azo analogues of BR could pump protons (because a membrane fragment containing the azo chromophore–bound bacterioopsin was used to test the pH changes). Moreover, the author have observed that the azo chromophore Az I– and Az II–bound POP could not pump protons and did not undergo any pH changes upon illumination. Accordingly, the author characterized the photochemical reactions and investigated the proton pumping functions of azo analogues of BR. Incubation of bacterioopsin with the azo chromophores yielded BAz I and BAz II, which exhibited orange pigmentation (Fig. 2.12A). The apomembrane containing bacterioopsin protein (BOP) prepared for reconstitution of the azo chromophore, did not display the UV–Vis absorption signals of the retinal pigment or retinal oxime (Fig. 12B), indicating complete removal of the retinal unit. The purified azo-BOP complexes were characterized

in terms of their UV–Vis absorption bands (Fig. 2.12B). The formation of the azo-BOP complexes led to bathochromic shifts of the absorption bands: from 412 to 458 nm for Az I in BAz I and from 387 to 462 nm for Az II in BAz II (Table 2.1). These bathochromic shifts of the absorption bands of BAz I and BAz II, much like those of the *n*-butyl Schiff bases of the azo chromophores, confirmed the binding of the azo chromophores with BOP, presumably through the Schiff base to the Lys216 residue in the G helix. Nevertheless, the blue-shifts of the absorption bands of BAz I and BAz II, relative to the signals of the protonated *n*-butyl Schiff bases of the azo chromophore, suggested that the Schiff bases of BAz I and BAz II were not protonated in the dark state.

2.7 Photoinduced proton pumping and proton transfer of BAz I and BAz II

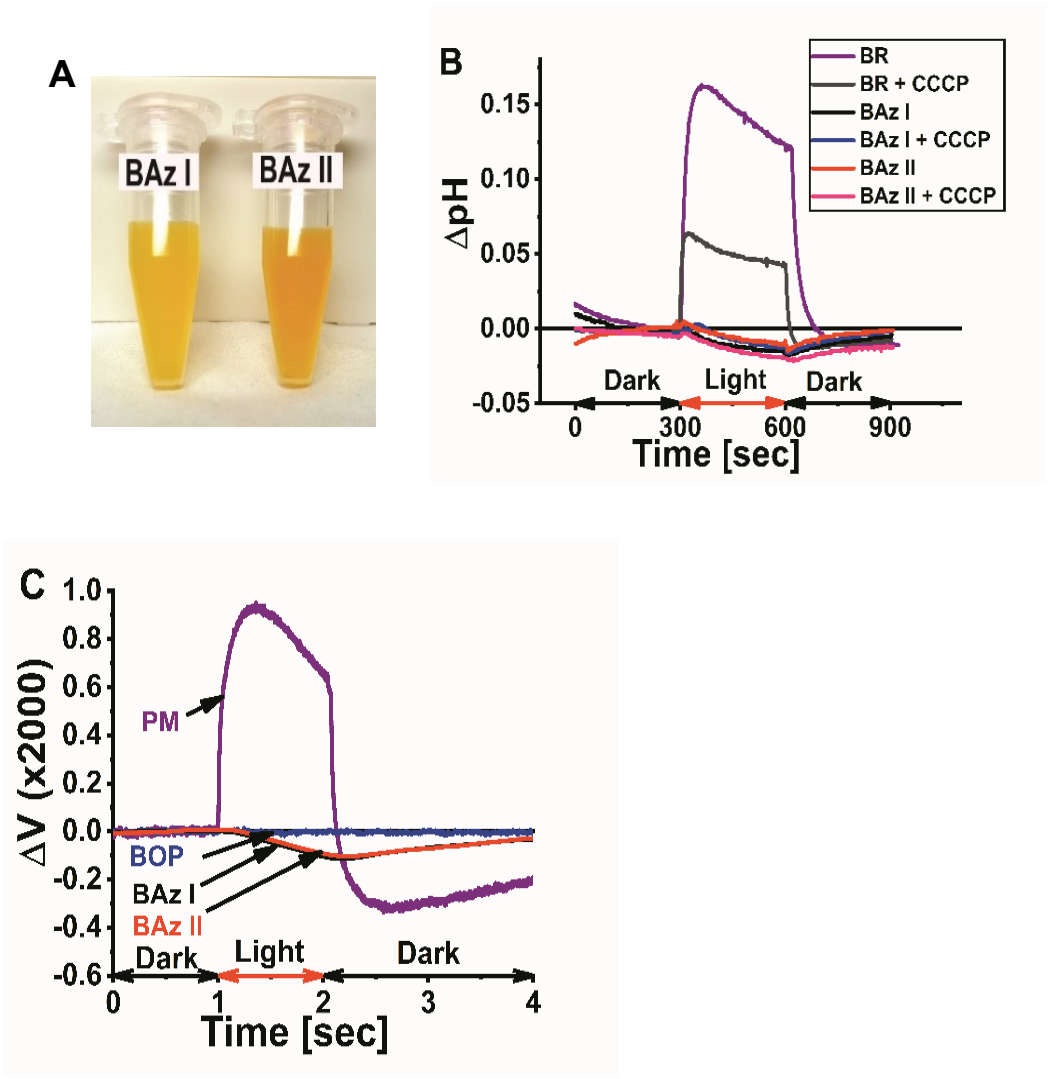

Fig. 2.13 Photoinduced proton-pumping and proton transfer of BAz I and BAz II. **A.** Photograph of Egg-PC reconstituted BAz I and BAz II. **B.** Photoinduced pH changes of Egg-PC reconstituted wild-type BR, BAz I, and BAz II, in the presence and absence of CCCP. **C.** Photoinduced potential changes of PM, BAz I, and BAz II.

To investigate the photoinduced proton pumping function, the author reconstituted BAz I and BAz II in PC liposomes; the retained color (Fig. 2.13A) implied successful reconstitution. As a positive control, the author also prepared the PC-reconstituted wild-type BR. The pigments were reconstituted in PC through a detergent-mediated reconstitution procedure, which led to their oriented reconstitution in the membrane.[32] Moreover, many microbial rhodopsins are known to undergo incorporation into liposomes with an inverted topology.[33] Reflecting this topology, the wild-type BR increased the pH of the suspension upon illumination; this pH change was impaired upon addition of CCCP (Fig. 2.13B), indicative of photoinduced inward proton pumping. On the other hand, BAz I and BAz II did not induce any pH changes, in either the presence or absence of CCCP, upon illumination (Fig. 2.13B). Thus, BAz I and BAz II could not pump the proton upon illumination. It has been reported previously that purple membrane (PM) induces such a pH change upon illumination.[12] Thus, the author investigated the photoinduced pH change of PM, without reconstitution in PC, under similar conditions. PM did not change the pH of the suspension upon illumination, consistent with speedy release and uptake of the proton in the same salt solution upon illumination (data not shown).

The author used a photoelectrochemical cell featuring ITO electrodes to study the photoinduced proton transfers of PM, BAz I, and BAz II. As a positive control, testing PM led to a positive potential change upon illumination, indicating initial release of the proton followed by proton uptake (Fig. 2.13C).[15] The proton transfer reaction of the wild-type BR followed a sequence different from that of the wild-type PR, due to presence of a proton-releasing group at the EC side.[34,35]

For wild-type BR, the upward and downward deflections of the proton transfer signal of PM were indicative of initial release of the proton from the proton-releasing group and subsequent uptake of the proton from the CP side via the proton-donor residue D96, which corresponds to the E108 residue of wild-type PR. For wild-type BR, the photoinduced potential changes of PM appeared and disappeared upon switching the light on and off, respectively, consistent with a very fast photoreaction. Interestingly, BAz I and BAz II experienced potential changes upon illumination that were indicative of photoinduced proton transfer occurring initially with proton uptake and subsequently with proton release—the reverse of the sequence of the wild-type BR. Therefore, no proton pumping of BAz I and BAz II would be possible for proton circulation at the EC side upon illumination. The negative control sample BOP did not experience any photoinduced change in potential, indicating no contamination of wild-type BR and no artifacts. The proton transfer reactions of the azo analogues of BR were essentially identical to those of PAz I and PAz II.

2.8 Photochemical reaction of BAz I and BAz II

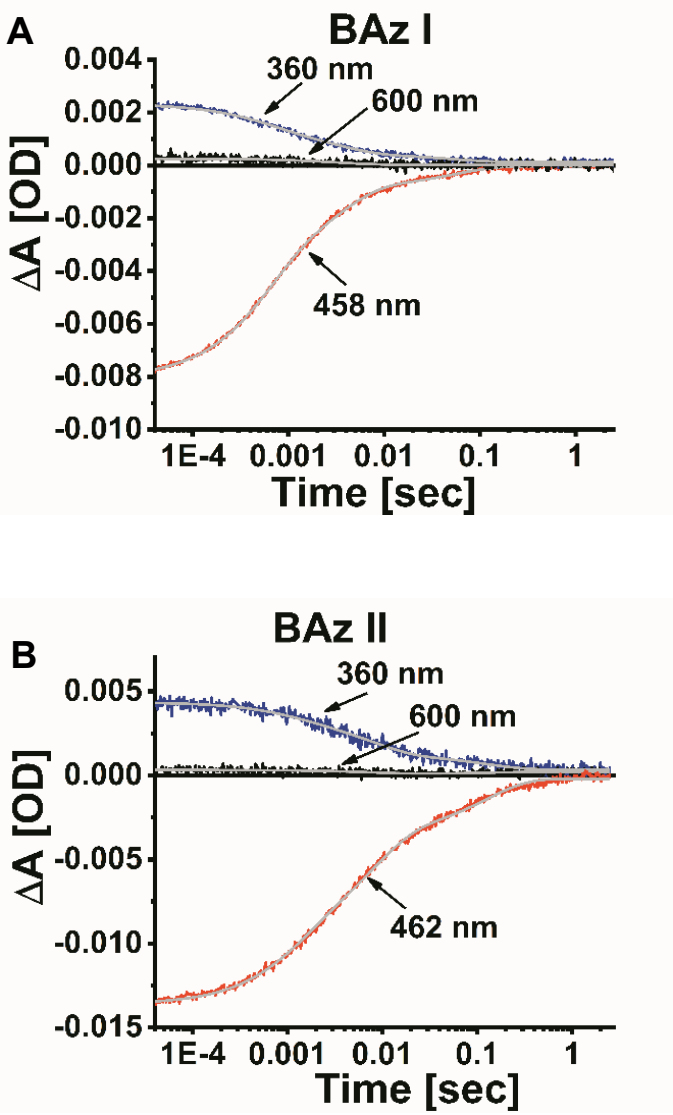

Fig. 2.14 Flash photolysis studies of BAz I and BAz II. Experimental and simulated flash-photolysis curves of BAz I **(A)** and BAz II **(B)** at three characteristic wavelengths (360, 458, and 600 nm). Fitting curves are provided in light gray.

The author used flash photolysis to study the photochemical reactions of BAz I and BAz II (Fig. 2.14A and Fig. 2.14B), respectively). Both BAz I and BAz II experienced flash-induced changes in their transient absorptions and thermal recoveries within 1.0 s at their characteristic values of λ_{max}. Moreover, both BAz I and BAz II underwent increases in the transient absorbance at 360 and 600 nm. These data are consistent with the cyclic photoreactions of BAz I and BAz II. The slower cyclic photoreactions of BAz I and BAz II, relative to those of the azo chromophores Az I and Az II, also confirmed that interactions existed between the azo chromophore units and the BOP. To investigate the photoreaction kinetics of BAz I and BAz II, the author fitted the flash photolysis curves of BAz I and BAz II at various wavelengths by employing the same sequential reaction model and equations used for PAz I and PAz II. Indeed, the flash photolysis curves of BAz I and BAz II at the three wavelengths were fitted well. Table 2.43 (for BAz I) and Table 2.5 (for BAz II) list the decay rate constants of the three transient steps, the molar absorptivities of the four species, and the values of RSS at the various wavelengths. Fig. 2.15 summarizes the photoreaction kinetics of BAz I as a typical example. In case of BAz I, the thermal decay rate constants of the three transient steps were 1.76×10^3, 311.1, and 18.57 s^{-1}. Upon formation of intermediate P_1, the molar absorptivity of BAz I increased significantly at 360 nm (6.0×10^3 M^{-1} cm^{-1}) and 600 nm (800.76 M^{-1} cm^{-1}), but decreased sharply at 458 nm (143.40 M^{-1} cm^{-1}) when compared with the initial state P_0. Subsequently, formation of the intermediate P_2 increased the molar absorptivity at 458 nm (1.24×10^4 M^{-1} cm^{-1}), but decreased it at 360 nm (3.19×10^3 M^{-1} cm^{-1}) and 600 nm (694.84 M^{-1} cm^{-1}), relative to those of the intermediate P_1. Thereafter, forming the intermediate P_3 led to a further increase

in the molar absorptivity at 458 nm (1.88×10^4 M^{-1} cm^{-1}), but decreases at 360 nm (1.05×10^3 M^{-1} cm^{-1}) and 600 nm (71.87 M^{-1} cm^{-1}), when compared with those of P_2. The simulated molar absorptivities of the initial state P_0 at wavelengths of 458, 360, and 600 nm were 2.08×10^4, 315.43, and 78.09 M^{-1} cm^{-1}, respectively; that is, they were reasonably close to the experimental values. The author observed similar photoreaction kinetics in the case of BAz II. These data strongly suggest that, upon illumination, BAz I and BAz II undergo cyclic photoreactions that feature three transient species. This flash photolysis analysis also implies that the photochemical reactions of BAz I and BAz II were identical to those of PAz I and PAz II.

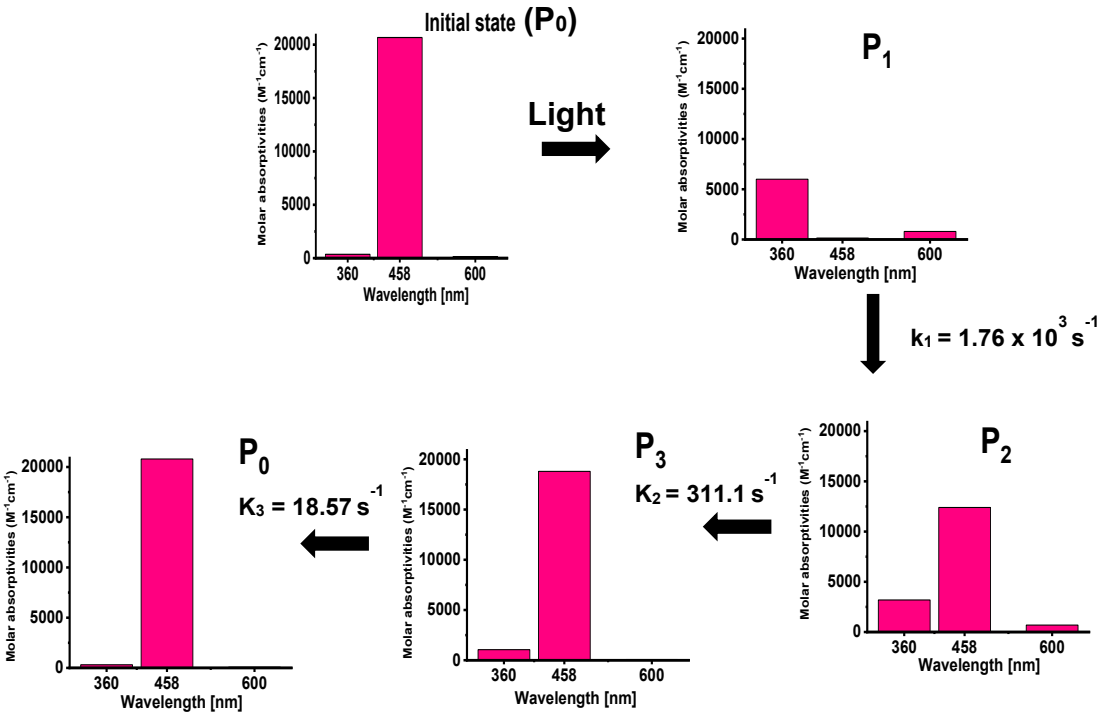

Fig. 2.15 As a typical example, schematic presentation of formation of different transient intermediates along with their molar absorptivity changes at different wavelength during photoreaction of BAz I.

Table 2.4 Fitting parameters of the flash photolysis data of BAz I recorded at 458, 360, and 600 nm.

Wave-length (nm)	k_1 (s^{-1})	k_2 (s^{-1})	k_3 (s^{-1})	ϵP_1 (M^{-1} cm^{-1})	ϵP_2 (M^{-1} cm^{-1})	ϵP_3 (M^{-1} cm^{-1})	ϵP_0 (M^{-1} cm^{-1})	RSS
458	1.76×10^3 ± 33.0	311.1 ± 11.0	18.57 ± 0.98	143.4 ± 19.0	1.24×10^4 ± 156.0	1.88×10^4 ± 57.0	2.08×10^4 ± 15.0	2.21×10^{-6}
360	1.76×10^3	311.1	18.57	6.0×10^3 ± 18.0	3.19×10^3 ± 34.0	1.05×10^3 ± 25.0	315.43 ± 15.0	2.94×10^{-6}
600	1.76×10^3	311.1	18.57	800.8 ± 33.0	694.8 ± 61.0	71.87 ± 46.0	78.09 ± 28.0	6.37×10^{-6}

Table 2.5 Fitting parameters of the flash photolysis data of BAz II recorded at 462, 360, and 600 nm.

Wave-length (nm)	k_1 (s^{-1})	k_2 (s^{-1})	k_3 (s^{-1})	ϵP_1 (M^{-1} cm^{-1})	ϵP_2 (M^{-1} cm^{-1})	ϵP_3 (M^{-1} cm^{-1})	ϵP_0 (M^{-1} cm^{-1})	RSS
462	879.3 ± 40.0	127.1 ± 5.00	8.01 ± 0.30	614.5 ± 28.0	8.39×10^3 ± 239.0	1.74×10^4 ± 104.0	2.24×10^4 ± 32.0	1.59×10^{-6}
360	879.3	127.1	8.01	7.05×10^3 ± 33.0	5.06×10^3 ± 64.0	1.93×10^3 ± 53.0	549.3 ± 37.0	1.59×10^{-6}
600	879.3	127.1	8.01	509.5 ± 21.0	478.8 ± 41.0	132.4 ± 34.0	334.3 ± 24.0	1.31×10^{-6}

2.9 Formation and photo-induced proton transfer of BAz III

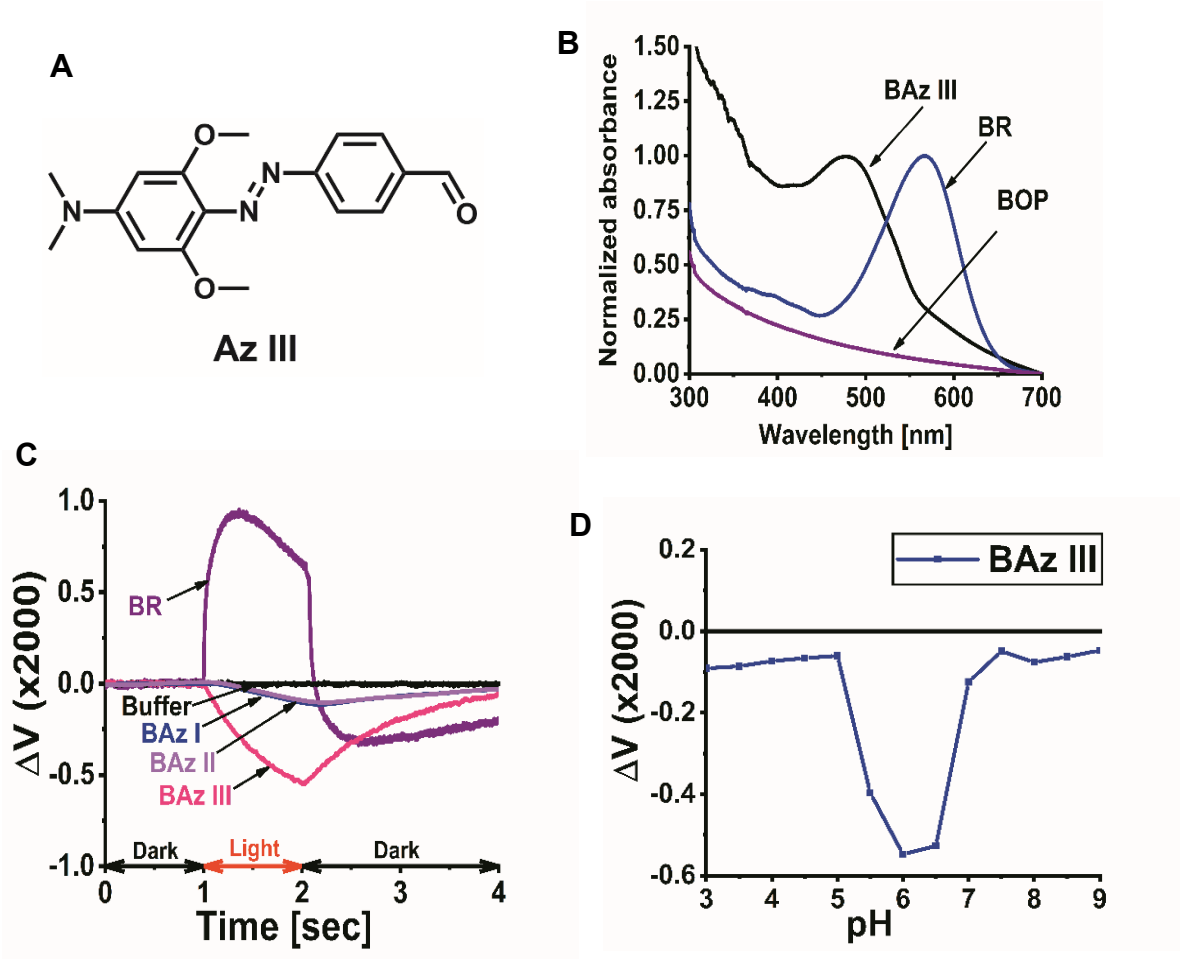

Fig. 2.16 Formation and characterization of bacteriorhodopsin analogues BAz III. **A.** Molecular structure of azo chromophore Az III. **B.** UV-vis absorption spectrum of BAz III (black line). **C.** Change in the photoinduced proton transfer potentials of BAz I (blue line), BAz II (magenta line), BAz III (pink line) and wild-type BR (purple line). **D.** pH-Dependent changes in the photoinduced proton transfer potentials of BAz III (blue line). Here, maximum photoinduced potential changes of BAz III upon illumination against pH were plotted.

To investigate the photofunctional properties of azo analogues BR and PR, another azo chromophore, having two ortho dimethoxy substitution in phenyl ring denoted as Az III (Fig. 2.16A), was designed and synthesized. According to previous report, ortho tetra-methoxy substitution in phenyl rings of azobenzene

leads to formation of azonium ion in neutral pH which undergoes decrease of basicity upon formation of transient cis isomer.[36] Azo chromophore Az III was designed in aim to provide the feature of formation of protonated Schiff base with opsin protein in dark state which would lead to proton release first upon photoisomerization. The interaction of azo chromophore Az III with BOP causes the red-shift of absorption band of Az III in BAz III from 464 to 483 nm (shown in Fig 2.16B), indicating the binding with azo chromophore with Lys216 residue of BOP presumably through the Schiff base. BAz III also showed the photoinduced potential change (shown in Fig. 2.16C), indicating its proton uptake first upon illumination, followed by proton release. This result indicates that even though, Az III has more electron pushing two ortho-dimethoxy substitution, Schiff base of BAz III is unprotonated in dark state and upon illumination BAz III underwent proton uptake first because of increasing of pKa value of Schiff base. BAz III showed the higher photo-induced proton transfer reaction in pH range 5.5 to 6.5 (shown in Fig. 2.16D), confirming its proton transfer reaction. However, Az III bound proteorhodopsin analogues PAz III, (UV-vis λ_{max} is 485 nm) showed the proton-transfer reaction similar to that of PAz I and PAz II (data not shown). However, BAz III could not be reconstituted in Egg-PC to form vesicle for proton pumping test. It was found that during the dialysis as a part of reconstitution in lipid, decomposition of BAz III was observed. Therefore, further modification of reconstitution process for BAz III is needed in order to confirm the proton pumping test. Moreover, like other azo analogues, BAz III undergoes proton uptake and release from same extra cellular side. Interestingly, BAz III showed higher potential change upon illumination compared to BAz I and BAz II (Fig. 2.16C). Higher proton transfer reaction of BAz III might be explained by the

increasing of basicity difference upon illumination due to presence of more electron donating methoxy substituent in Az III which may increase the electron density in Schiff base result in increasing of proton acceptance affinity. It was found that all three azo analogues of PR showed almost similar potential changes in proton transfer reaction upon illumination. Higher efficiency of BAz III may indicate that compared to POP protein, extracellular channel of BOP is more hydrophobic.

2.10 Putative mechanism of photoinduced proton transfer of azo analogues of PR and BR

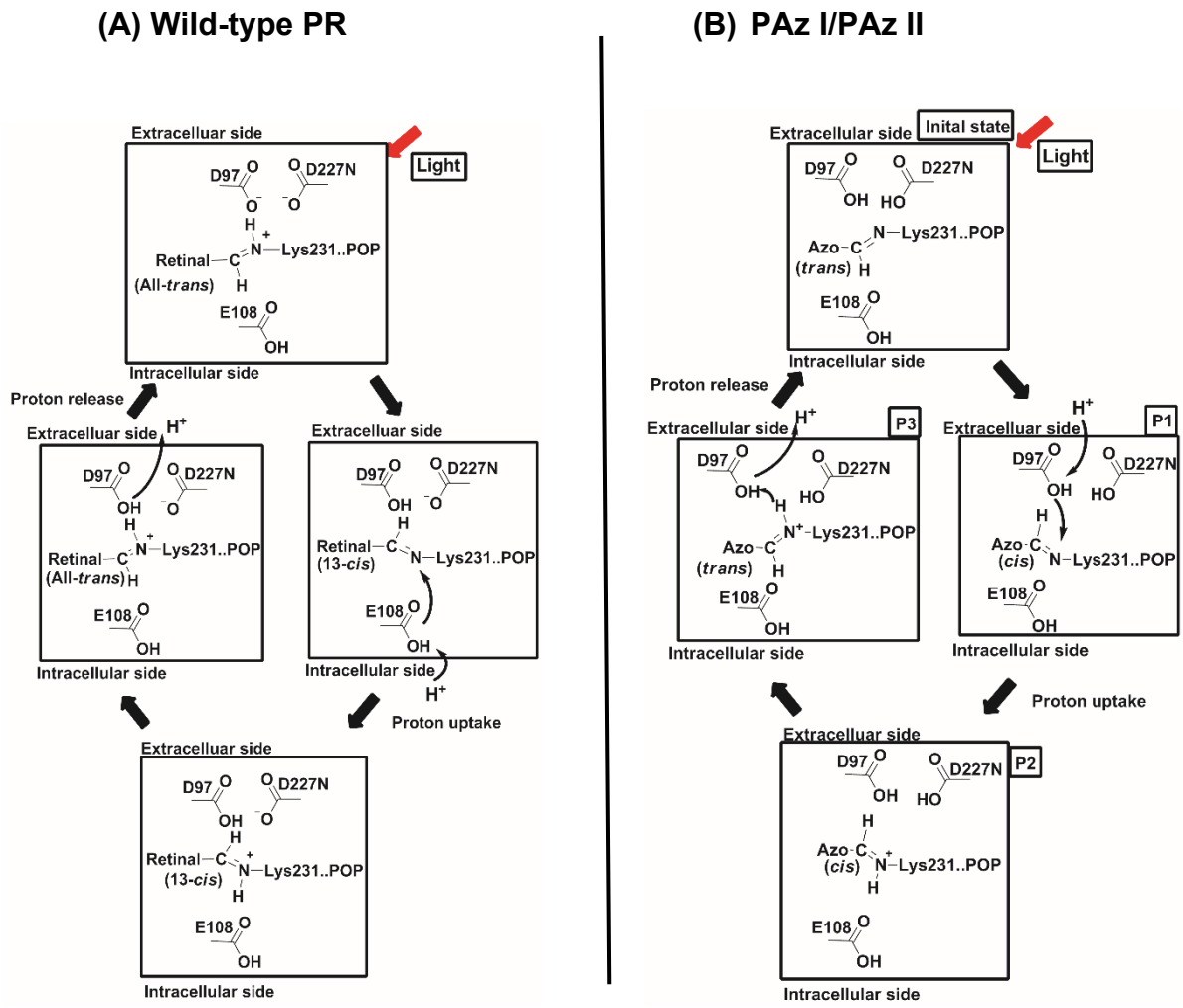

Fig. 2.17 Putative mechanism for proton transfer during photocycling of azo analogues of PR and BR. **A.** As a typical example, putative mechanism for photoinduced proton transfer of PAz I/PAz II. **B.** Mechanism of photoinduced proton transfer of wild-type PR.

Based on our new results described herein and previous findings, the author has developed a mechanism for the photoinduced proton transfer processes of the azo analogues of PR and BR. Here, the author proposes a putative model of the structural changes and proton movements during the photocycles of the azo analogues of PR and BR. As a typical example, Fig. 2.17A displays the mechanism for the proton transfer of wild-type PR; Fig. 2.17B presents the structures and structural changes of PAz I and PAz II. The proton transfer reactions of the azo analogues of PR and BR were entirely different from that of the wild-type PR/BR. Upon illumination, the wild-type PR underwent proton transfer in the following order: transfer of a proton from the protonated Schiff base to Asp97, uptake of the proton from the CP side via the Glu108 residue, and release of the proton from the Asp97 residue to the EC side. On the other hand, UV–Vis spectral analysis revealed that the Schiff base in PAz I was not protonated in the initial state. Furthermore, the azo chromophore Az I unit in PAz I would exist in the *trans* state in the dark, due to the stability of the *trans* azo chromophore being higher than that of the *cis* form.[37] Mutational studies suggested that the Schiff base of PAz I interacted with nearby negatively charged carboxyl ions of the D97 and D227 residues. Flash-induced depletion of the initial state and thermal recovery manifested repeated cycles of the reversible *trans*/*cis* photoisomerization of the azo chromophore units in the azo-protein complexes. Flash photolysis analysis also revealed that, upon illumination, the *trans*-azo chromophore embedded in PAz I isomerized to the *cis* form, leading to the production of three spectroscopically distinct intermediates—**P1**, **P2** and **P3**—during the photocycle; Fig. 2.17A presents their proposed molecular structures.

Upon illumination, PAz I undergoes photoisomerization to form the intermediate **P1** within a picosecond time domain. The formation of **P1** was supported by blue-shifting of the absorption band from 448 nm to near 370 nm. This *trans*-to-*cis* isomerization of the azo chromophore increased the basicity of the Schiff base in **P1**. Mutational analysis confirmed that the amino acid residue E108 did not act as a proton donor in PAz I, suggesting that the Schiff base did not take up the proton from the CP side. Examination of the photoinduced proton transfer revealed that PAz I accepted the proton initially upon illumination. Mutational analysis suggested that PAz I might accept the proton from the nearby carboxylic acid group of residue D97. Therefore, upon formation of **P1**, PAz I may accept the proton from the EC side through D97, followed by the formation of the intermediate **P2**. Protonation of the Schiff base in **P2** was supported by the red-shifting of the absorption band from 370 nm to near 448 nm. The intermediate **P2** decays through thermal isomerization to give the intermediate **P3**. This *cis*-to-*trans* isomerization would decrease the pK_a of the Schiff base. As a result, the intermediate **P3** releases the proton to the EC medium, presumably via residue D97, and return to its initial state. The photoinduced proton transfer reactions of PAz II, BAz I, and BAz II can be explained in terms of similar structural changes and photochemical phenomena.

3. Experimental

3.1 Synthesis of azo chromophores Az I and Az II

4-[[4´-(*N*,*N*-Dimethylamino)phenyl-1´]azo]benzaldehyde (Az I) and 3-[4-[[4´-(*N*,*N*-dimethylamino)phenyl-1´]azo]phenyl-1]prop-2-enal (Az II) were synthesized according to reported procedures.[12] The molecular structures of Az I and Az II are presented in Fig. 1.3. The azo chromophores Az I and Az II were characterized using ^{1}H and ^{13}C NMR spectroscopy (ECX-400, JEOL) (Figs. 3.1–3.4). and high-resolution mass spectrometry (ESI-TOF MS, JMS-T100CS, JEOL) (Figs. 3.7–3.8).

Az I: ^{1}H NMR (400 MHz, $CDCl_3$) δ 10.06 (s, 1H), 7.90–8.00 (m, 6H), 6.77 (d, J = 9.3 Hz, 2H), 3.12 (s, 6H). ^{13}C NMR (101 MHz, $CDCl_3$) δ 191.88, 157.00, 153.17, 143.87, 136.21, 130.82, 125.83, 122.74, 111.55, 40.39. HR-MS (ESI, *m*/*z*) calcd for $C_{15}H_{16}N_3O$ $[M + H]^+$: 254.12879; found: 254.12867 [observed error (–0.47 ppm) is within the range of the instrument error (±5.00 ppm)].

Az II: ^{1}H NMR (400 MHz, $CDCl_3$) δ 9.73 (d, J = 7.68 Hz, 1H), 7.87–7.91 (m, 4H), 7.68 (d, J = 8.6, 2H), 7.52 (d, J = 18, 1H), 6.73–6.79 (m, 3H), 3.11 (s, 6H). ^{13}C NMR (101 MHz, $CDCl_3$) δ 193.75, 154.94, 152.94, 152.23, 143.83, 134.60, 129.49, 128.73, 125.57, 122.96, 111.57, 40.40. HR-MS (ESI, *m*/*z*) calcd for $C_{17}H_{18}N_3O$ $[M + H]^+$: 280.14444; found: 280.14436 [observed error (–0.28 ppm) is within the range of the instrument error (±5.00 ppm)].

3.2 Synthesis of azo chromophore Az III

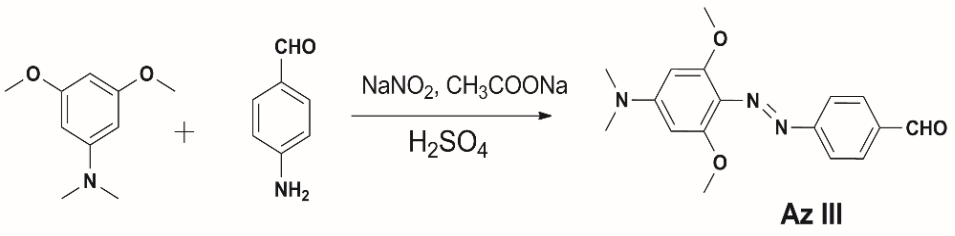

Scheme 3.1 Synthetic procedure of azo chromophore Az III

The synthetic procedure of the compound 4-[[2´,6´-dimethoxy, 4´-(N,N-dimethylamino)phenyl-1´]azo]-benzaldehyde (denoted Az III) was shown in Scheme 3.1. 4-Nitrobenzaldehyde was reduced to 4-aminobenzaldehyde by literature procedure.[38] 3,5-Dimethoxy-N,N-dimethylaniline was also synthesized by literature procedure.[39] Coupling of 3,5-Dimethoxy-N,N-dimethylaniline with the 4-aminobenzaldehyde was done using a slight modification of known procedure.[40] Sodium nitrile (116.25 mg, 1.65 mmol) was added in portions to 4 mL cold sulfuric acid, and the mixture was warmed gradually to 70 ˚C. After all of the sodium nitrite was dissolved, the mixture was cooled to 5 ˚C. Next, 200 mg (1.65 mmol) of 4-aminobenzaldehyde was added to the above solution. The mixture was stirred for 2 h at 5-10 ˚C and then poured into 15 g of ice-cold water. After filtration, the diazonium solution was added drop wise to corresponding N,N-dimethylaniline (1.65 mmol) in 3.5 mL 0.1N hydrochloric acid while maintaining the temperature at 10-15 ˚C. Next, 0.23 g of sodium acetate was added, after which the mixture was stirred at 10-15 ˚C for 12 h. After that, the mixture was brought to pH 8-9 with saturated sodium bicarbonate solution. The mixture was then extracted with ethyl acetate (3 × 50 mL). The combined organic phases were washed with 100 mL of brine, dried over Na_2SO_4, filtered and the

solvent was removed under reduce pressure to leave solids. The compound was purified by column chromatography over a silica gel column and characterized by ^{1}H-NMR, ^{13}C NMR, (Figs. 3.5-3.6) and HRMS (Fig. 3.9). 220 mg (42%) of dark orange red solid for azo chromophore Az III was obtained.

Az III: ^{1}H-NMR (400 MHz, $CDCl_3$), *δ* (ppm) : 10.03 (s, 1H, -CHO), 7.94 (d, 2H, *J* = 8.4 Hz 2H,6H-PhCHO), 7.89 (d, 2H, J = 8.2 Hz, 3H,5H-PhCHO), 5.90 (s, 2H, 3H,5H-PhNMe$_2$), 3.95 (s, 6H, -OMe$_2$), 3.14 (s, 6H, -NMe$_2$); ^{13}C NMR (400 MHz, $CDCl_3$) *δ* (ppm) : 192.1, 159.0, 157.3, 154.2, 135.5, 130.8, 124.7, 122.3, 88.6, 56.3, 40.4. HRMS ESI $[M+H]^+$: calcd for $C_{17}H_{20}O_3N_3$: 314.14992, found: 314.15006, [observed error (0.45 ppm) is within the range of the instrument error (±5.00 ppm)]

3.3 Azo-POP complexes and azo-POP mutant complexes

3.3.1 *Wild-type POP protein and three POP mutant proteins (POP-D97N, POP-D227N, and POP-E108Q)*

The wild-type POP-expression plasmid (pET-POP) was constructed by inserting the POP gene into Nde I/Xho I sites of pET-21c vector (Merck). The gene sequence was identical to that described in previous reports.[5,15] The resultant POP had an additional eight amino acids (–LEHHHHHH) at its C-terminus. This plasmid was used to transform *E. coli* BL21 (DE3) cells.[5,15] The expression plasmids of POP-D97N and POP-D227N, which were encoded in pBAD vector, have been reported previously.[16] Using the same method, the plasmid for POP-E108Q expression was constructed here. For expression of the mutants POP-D97N, POP-E108Q, and POP-D227N, plasmids (pBAD) were used to transform *E. coli* UT5600 cells.[15] The growth broths were 2 x YT

supplemented by ampicillin (final concentration: 50 μg mL^{-1}) and cultivated at 37 °C and 120 rpm until the OD at 660 nm reached 1.7–1.8. Next, 1 mM isopropyl *β*-D-(–)-thiogalactopyranoside (IPTG; for wild-type POP) or 0.2% L-(+)-arabinose (for the three mutants of POP) was added in the culture broth, and cultivation was continued at 37 °C for another 3–4 h. The cells were centrifuged (6000 rpm, 6 min, 4 °C) and the pellets suspended in Buffer A (50 mM Tris-HCl, pH 7.0, 5 mM $MgCl_2$). After suspending, the cells were washed in Buffer A through centrifugation and then disrupted through sonication. The cell debris was removed by additional centrifugation (8500 rpm, 4 °C, 10 min), and the membrane fraction was collected by ultra-centrifugation (40000 rpm, 4 °C, 1.5 h), followed by suspension in Buffer S [5 mM imidazole, 50 mM Tris-HCl (pH 8.0), and 300 mM NaCl]. The membrane was solubilized in Buffer S supplemented with 1.5% (w/v) of the detergent *n*-dodecyl-*β*-D-maltoside (DDM) with gentle stirring overnight in a cold room (4 °C); the unsolubilized portions were removed by ultra-centrifugation (40000 rpm, 4 °C, 1 h). The supernatants were applied to a Ni-NTA agarose (QIAGEN, Tokyo, Japan) column, and shaken gently for at least 45 min. Nonspecific materials were removed from the column by washing with Buffer W [50 mM imidazole, 50 mM Tris-HCl (pH 7.5), 0.05% DDM, 300 mM NaCl]. Elution of wild-type POP and the three mutant types of POP was performed using Buffer E [500 mM imidazole, 50 mM Tris-HCl (pH 7.0), 0.1% DDM, 300 mM NaCl]. Imidazole in protein solution was removed through dialysis against Buffer D [10 mM MOPS (pH 7.0), 0.1 M NaCl, 0.05% DDM] at 4 °C for 3 days (every 12 h, 0.5 L). For the positive control, wild-type PR protein was prepared using plasmid (pET-POP) transformed into *E. coli* BL21 (DE3) cells and following the procedures described above; in addition, 10 μM all-*trans* retinal

(Sigma–Aldrich, St. Louis, MO, USA) and IPTG were added in the culture broth.[5,15] SDS-PAGE revealed main thick bands of wild-type POP, the three mutant types of POP, and the wild-type PR near 25 kDa. The purified protein samples were characterized through UV–Vis spectral analysis using a UV-1800 spectrometer (Shimadzu, Kyoto, Japan). The amounts of wild-type POP and the mutants POP-D97N, POP-E108Q, and POP-D227N were estimated using a molar extinction coefficient (ϵ) of 65000 M^{-1} cm^{-1} at 280 nm. The value of ϵ of the POP protein at 280 nm was calculated from the UV–Vis absorption spectrum of PR; a value of ϵ of 50,000 M^{-1} cm^{-1} was used for PR at 520 nm. To calculate the value of ϵ at 280 nm, the base line shifting due to scattering was subtracted from the experimental absorbance.

3.3.2 *Azo analogues of wild-type PR and PR mutants*

The azo chromophores Az I and Az II were dissolved in EtOH and DMSO, respectively. The azo chromophores Az I and Az II were incubated with POP (0.1 mM) in an aqueous medium at pH 7 (10 mM MOPS, 0.1 M NaCl, 0.05% DDM) under continuous gentle shaking at room temperature in the dark for 24 h. The concentration of each azo chromophore was 0.45 mM. The final concentrations of EtOH and DMSO in their respective protein suspensions were approximately 3.5% (v/v). After 24 h, the reaction mixtures were added into Ni-NTA agarose columns and shaken at room temperature for 0.5 h. After adsorption of the azo-POP complexes, nonspecific materials were removed from the columns by washing initially with wash Buffer 1 [50 mM Tris-HCl (pH 7.0), 0.1 M NaCl, 20 mM imidazole, 2% bovine serum albumin (BSA), 0.1% (v/v) Triton X-100] and

then with wash Buffer 2 [50 mM Tris-HCl (pH 7.0), 0.1 M NaCl, 20 mM imidazole, 0.1% DDM]. Elution of the azo-POP complexes was performed using Buffer E. The imidazole in the azo-POP complex solutions was removed through dialysis against Buffer D at 4 °C for 3 days. The SDS-PAGE bands of the azo analogues of PR had the same molecular weight as the wild-type PR (Figs. 3.10 and 3.11), confirming their purity. The purified azo-POP complexes were characterized through UV–Vis spectral analysis. The value of ϵ at λ_{max} was calculated by using the value of ϵ of the POP protein at 280 nm (65,000 M^{-1} cm^{-1}). The values of ϵ of PAz I and PAz II at λ_{max} were 25,380 and 20,762 M^{-1} cm^{-1}. The solutions of the azo-POP complexes were stored at 4 °C. The azo analogues of the mutant proteins POP-D97N, POP-E108Q, and POP-D227N were prepared similarly, following the method described above. The SDS-PAGE bands of the azo analogues of the POP mutant proteins had the same molecular weight as the wild-type PR (Figs. 3.10 and 3.11).

3.4 Azo-bacterioopsin complexes

3.4.1 *Bacterioopsin protein (BOP)*

Purple membrane (PM) fragments were isolated and purified from the *H. salinarum* strain ET1001 using the general method.[41] To obtain bacterioopsin, removal of the retinal from PM was accomplished by modification of the general method.[42] This general method led to an intact apomembrane (BOP) that could be used to regenerate an analogue of the native membrane; nevertheless, the residual absorption at 360 nm, even after washing, suggested that some retinal oxime or free retinal remained in the membrane. Some thermal or photocatalyzed *cis–trans* isomerization of the free retinal or retinal-oxime may

have occurred.[43] Even the presence of retinal oxime or free retinal could interfere with the binding of the artificial chromophore and also regenerate the native member. Therefore, to ensure complete removal of the retinal-oxime or free retinal, 2% (v/v) Tween 20 was added in the bleach buffer and wash buffer. To remove retinal, PM was added in the bleach buffer [50 mM Tris-HCl (pH 7), 2 M hydroxylamine, 0.1 M NaCl, 2% (v/v) Tween 20] and subjected to irradiation with yellow light (>460 nm, Toshiba) under continuous stirring for 4 h at RT. After bleaching, the hydroxylamine and retinal oxime were washed out using wash buffer [50 mM Tris-HCl (pH 7.0), 0.1 M NaCl, 2% BSA, 2% (v/v) Tween 20], stirring for 5 min, and centrifugation (40,000 rpm, 0.5 h, 4 °C). This step was repeated four times. To remove BSA, the membrane was suspended in Buffer R [10 mM Tris-HCl, 0.1 M NaCl (pH 7.0)] and centrifuged (40,000 rpm, 4 °C, 0.5 h). This step was repeated twice. Finally, the solid precipitate of BOP was suspended in Buffer R and stored at 4 °C. The purity of obtained BOP was confirmed by UV–Vis spectral analysis and flash photolysis at high concentration. The purified PM and BOP also appeared as SDS-PAGE bands near 26 kDa (Fig. 3.12). The amount of BOP was estimated using a molar extinction coefficient of 93,000 M^{-1} cm^{-1} at 280 nm; this molar extinction coefficient of BOP was calculated from the UV–Vis absorption spectrum and using a value of ϵ of 63,000 $M^{-1}cm^{-1}$ at 570 nm for the wild-type BR. To calculate the value of ϵ at 280 nm, base line shifting due to scattering was subtracted from the experimental value.

3.4.2 *Azo analogues of bacteriorhodopsin*

The azo analogues of BR were prepared through modification of the reported method.[12] Solution of azo chromophores were added gradually to a suspension of BOP (4.0×10^{-5} M) in buffer R with gentle shaking. The mixtures were incubated at ambient temperature in the dark under continuous mild shaking for 24 h. The final concentration of azo chromophores was 1.5×10^{-4} M; the final EtOH and DMSO concentration were 3% v/v. After 24 h of incubation, the mixtures were diluted 20-fold with wash buffer [50 mM Tris-HCl, 0.1 M NaCl, 1% BSA (pH 7.0)], stirred for 5 min, and then centrifuged (40,000 rpm, 0.5 h, and 4.0 ˚C). This step was repeated three times. To remove BSA, the solids were suspended in Buffer R and centrifuged (40,000 rpm, 0.5 h, and 4.0 ˚C). This step was repeated twice. Finally, solids of azo-BOP complexes were resuspended in Buffer R. The SDS-PAGE bands of the purified azo-BOP complexes revealed that they had the same molecular weight as the wild-type BR (Fig. 3.12). The suspensions of azo analogues of BR were stored at 4 ˚C. The value of ϵ of BAz I, BAz II and BAz III at λ_{max} were 20,670 $M^{-1}cm^{-1}$, 22,281 $M^{-1}cm^{-1}$ and 25,300 $M^{-1}cm^{-1}$ respectively which were calculated using the value of ϵ BOP at 280 nm (93000 $M^{-1}cm^{-1}$).

3.5 Proton transfer reaction of azo analogues of PR, PR mutants and BR

3.5.1 *Sample Preparation*

Purified azo analogues of the wild-type PR and PR mutants were reconstituted in L-α-phosphatidylcholine (PC) from egg yolk (Avanti) according to the previously reported method.[15] Reconstitution of the azo analogues of the wild-type PR and PR mutants into PC was performed at a molar ratio of 1:50 (pigment:PC). The detergent from the reconstituted pigments was removed through dialysis in the presence of SM2 adsorbent Bio-beads (BIO-RAD, Hercules, CA) for 3 days at 4 °C. The Egg-PC reconstituted azo analogues of PR and the PR mutants were washed with distilled water through centrifugation (15,000 rpm, 5 min, 4 °C). This washing step was repeated three times. Finally, the pellets were suspended in distilled water (100 μL). Similarly, wild-type PR was reconstituted in PC. BAz I, BAz II, BAz III and wild-type BR were also prepared according to the procedure described previously.[15] To remove the buffer media, BAz I, BAz II and BAz III suspensions were centrifuged (40,000 rpm, 4 ˚C, 0.5 h), and resuspended with distilled water. This step was repeated two times. Finally, the pellets of them were suspended with distilled water. For wild-type BR, PM suspended in distilled water was used.

3.5.2 *Photochemical cell*

The construction of the photochemical cell was performed according to the literature.[15,44,45] The structure of the cell was as follows: working ITO electrode (covered with pigment)/100 mM NaCl + buffer components/ITO (reference electrode). A suspension (100 µL) of each Egg-PC–reconstituted azo analogue of wild-type PR or PR mutant or wild-type PR was adsorbed on the surface of a transparent ITO electrode under reduced pressure. Similarly, 100-µL suspensions of the azo analogues of BR and PM were adsorbed on the surface of an ITO electrode. To eliminate any unbound or weakly bound proteins, the electrode was cleaned with distilled water. The photochemical measurement with the ITO electrode was conducted at various values of pH from 3 and 9. To ensure a constant buffer capacity over this wide pH range, 6-mixed buffer solution was used, composed of citrate (1.37 mM), ADA (0.46 mM), TAPS (1.25 mM), MOPS (1.04 mM), CHES (0.81 mM), and CAPS (1.39 mM).

3.5.3 *Photoinduced proton transfer reaction*

These experiments were performed following previously reported procedures.[15,44] The light source for the excitation of the azo analogues of wild-type PR/BR and PR mutant analogues adsorbed on ITO electrode was a 150-W Xe arc in combination with an IR cutoff filter (IR-25S, Toshiba) and a cutoff optical filter L39 (Toshiba). For the wild-type PR, a cutoff optical filter L43 (Toshiba) was used; for the wild-type BR, Y46 (Toshiba) and a cutoff infrared filter (IR-25S, Toshiba) were used. Changes in the photoinduced potential were measured using a homemade amplifier. The duration of illumination was 1 s, adjusted by the mechanical shutter. Each transient signal was accumulated 10 times and

averaged to improve the baseline shift. The experiments were conducted at RT (ca. 25 °C).

3.6 Photoinduced proton pumping function of azo analogues of PR and BR

3.6.1 *Expression of azo analogues of PR and wild-type PR in E. coli cells*

The wild-type POP-expression plasmid (pET-POP) was used to transform *E. coli* BL21 (DE3) cells.[5,15] The cells were grown in 2 x YT medium supplemented by ampicillin (final concentrated of ampicillin: 50 μg mL^{-1}). Then cells were cultivated at 37 °C until the OD_{660} reached 1.0–1.2. Induction was started by the addition of 1 mM IPTG and 10 μM azo chromophore (Az I or Az II) or retinal; cultivation was continued for another 4 h. The cells were harvested through centrifugation (5500 rpm, 4 °C) and then washed with salt solution A (200 mM NaCl, 10 mM $MgCl_2 \cdot 6H_20$). The washing process was repeated three times. The cells in the salt solution A were starved overnight at 4 °C. Finally, the cells were suspended in salt solution A and their OD at 660 nm was adjusted to 10.0. As a control sample, *E. coli* BL21 (DE3) harboring pET-21c (POP unexpressed plasmid) was grown, incubated with 10 μM azo chromophore (Az I or Az II), and harvested using the same procedure as described above.

3.6.2 *Reconstitution of azo analogues of BR in Egg-PC liposome*

To form vesicles, the azo analogues of BR and wild-type BR were reconstituted in PC from egg yolk according to a previously described method.[33]

PC dissolved in $CHCl_3$ (20 mg mL^{-1}) was dried in a glass vial under a N_2 stream, followed by vacuum drying for 2–3 h. The dried PC was resuspended in 0.15 M KCl supplemented with 20% (w/v) sodium cholate. The azo analogues of BR and wild-type BR were added in the apparent suspension of PC at a ratio of 1:20 (w/w) and then the mixture was mildly shaken for 1 h. The sodium cholate was removed through dialysis against 0.15 M KCl for 3–4 days at 20 °C (every 12 h, 500 mL of solvent was changed). The final concentration of PC in the suspension was 2% (w/v).

3.6.3 *Photoinduced proton pumping function*

The light source was a 150-W Xe lamp with an IR filter (IR25S, Toshiba, Tokyo). Appropriate cutoff optical filters, as mentioned above, were used to excite the pigments. The distance between the Xe lamp and the sample was approximately 15 cm. The change in pH was monitored using a pH meter (model F-72; HORIBA, Japan). A cuvette having a thickness of 3.0 mm was used. The volume of the samples was 200 µL. The proton pumping function was tested in the presence and absence of CCCP (20 µM). The experiments were conducted at RT (ca. 25 °C) and in a dark room.

3.7 Flash photolysis of azo chromophores and azo analogues of wild-type PR, BR and PR mutants

Solutions of the azo analogues of wild-type PR and the PR mutants in buffer [10 mM MOPS (pH 7.0), 0.1 M NaCl, 0.05% DDM] were used for the flash photolysis studies. Solutions of Az I and Az II in aqueous buffer [10 mM MOPS

buffer (pH 7.0)] were used for their flash photolysis studies. Suspensions of BAz I and BAz II in pH 7.0 buffer (10 mM Tris-HCl, 0.1 M NaCl) were used for their flash photolysis studies. The OD at the characteristic value of λ_{max} of the azo pigments of the wild-type PR, BR, and PR mutants and of the azo chromophores were in the range 0.5–1.0. The apparatus and procedure for flash photolysis were the same as those reported previously.[46] The changes in transient absorbance induced by a laser pulse (Nd:YAG, 532 nm, 7 ns, 5 mJ pulse^{-1}) were acquired by a computer at intervals of 0.5 μs. The data acquired prior to the laser pulse were used as a baseline. Transient time-resolved absorption changes were obtained at various wavelengths. At each wavelength, the data from 100 laser pulses were averaged to improve the signal-to-noise ratio. A constant temperature of 25 °C was maintained using a thermostat (NCB-1200; Eyela). After measurement, the reproducibility of the data was checked to confirm that the sample had not denatured during the process. Curve fitting of the flash photolysis data was performed using the derived kinetic equations programmed into Origin-Pro 2018 software (OriginLab).

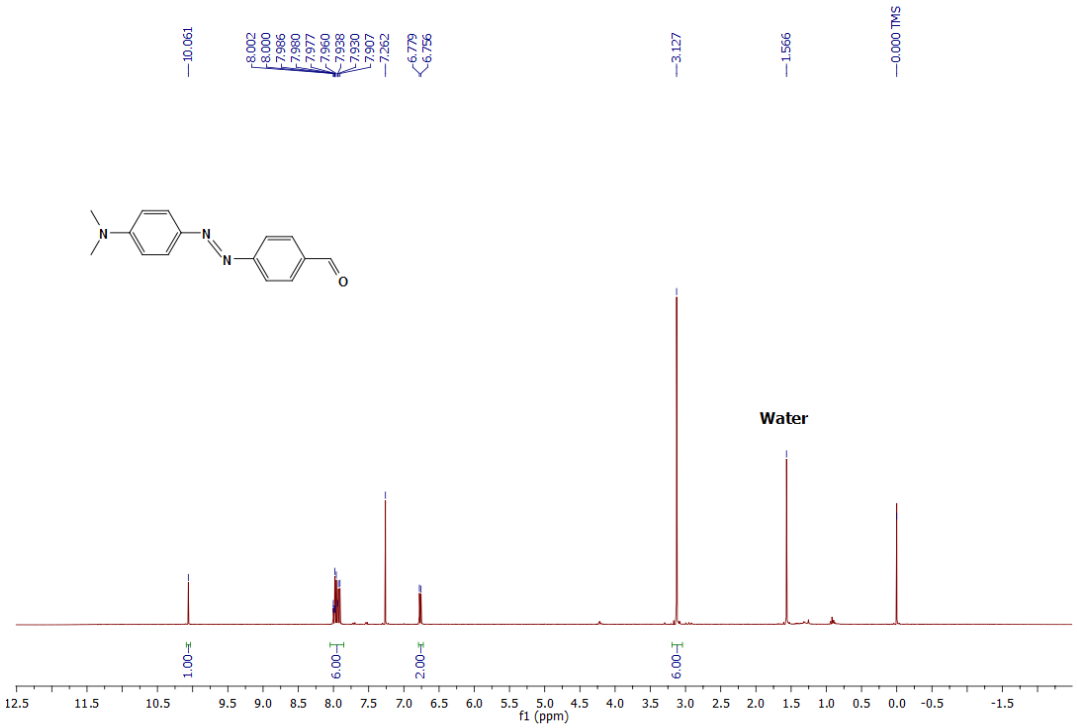

Fig. 3.1 ^{1}H NMR of Az I

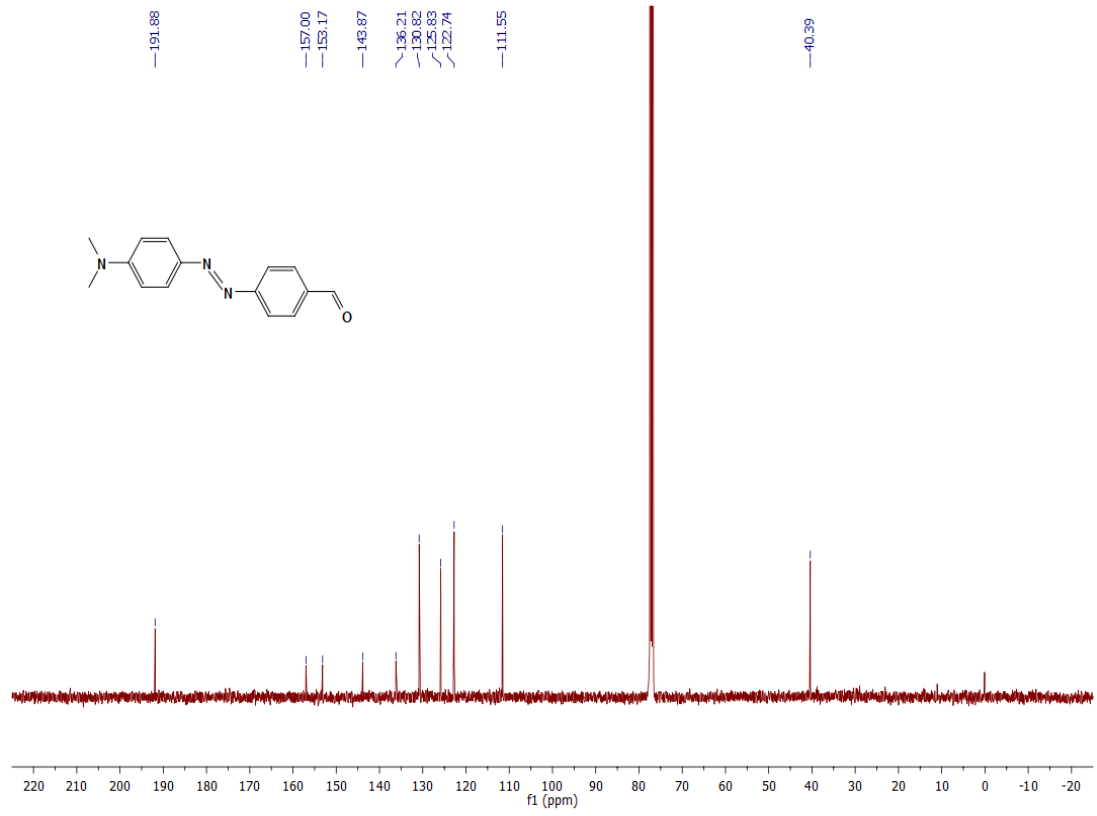

Fig. 3.2 ^{13}C NMR of Az I

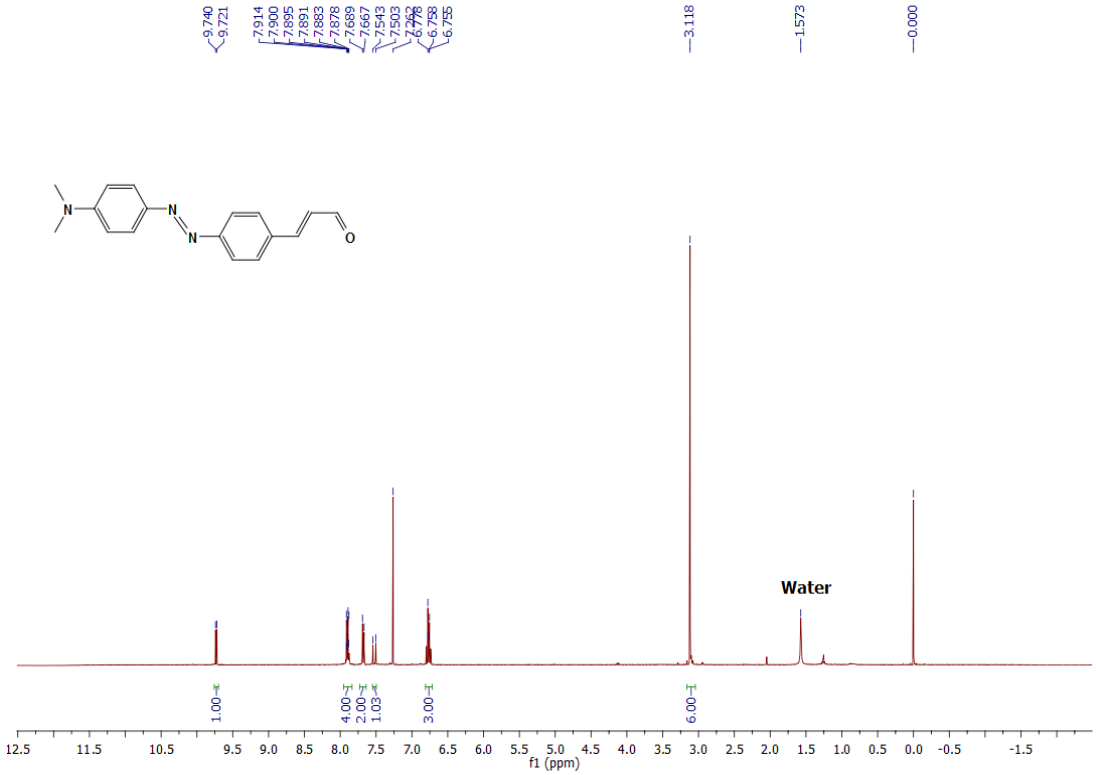

Fig. 3.3 ^{1}H NMR of Az II

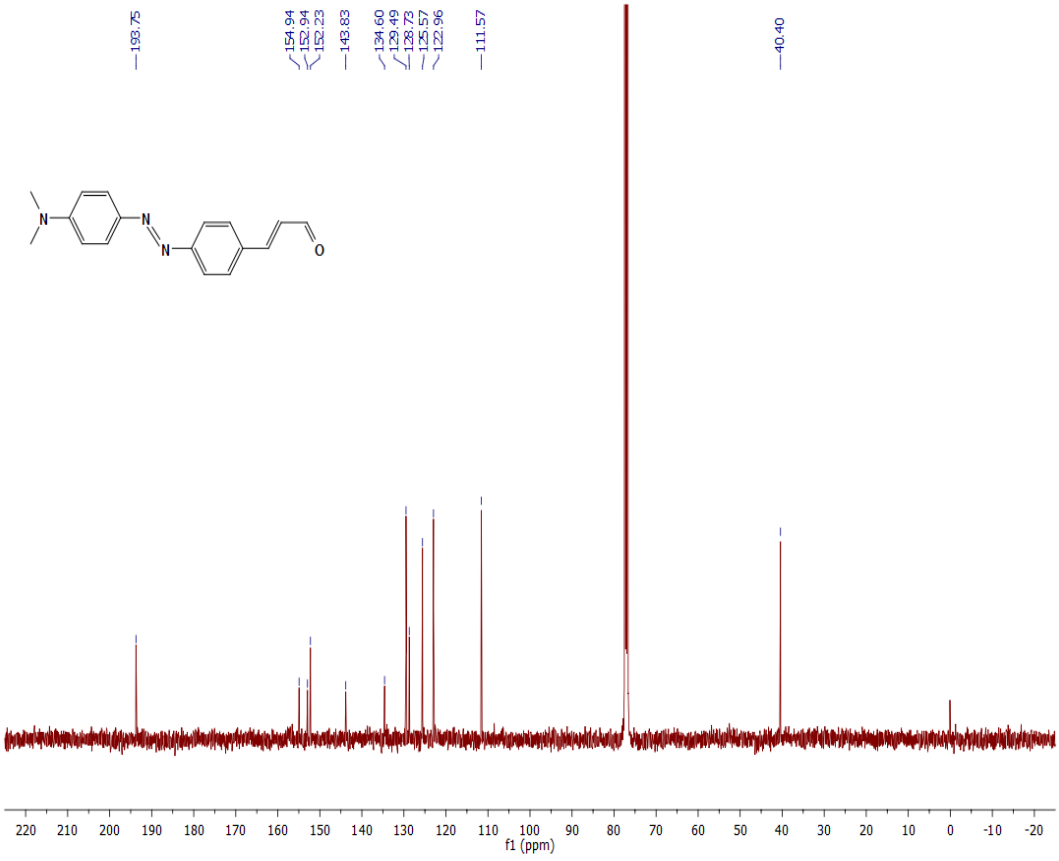

Fig. 3.4 ^{13}C NMR of Az II

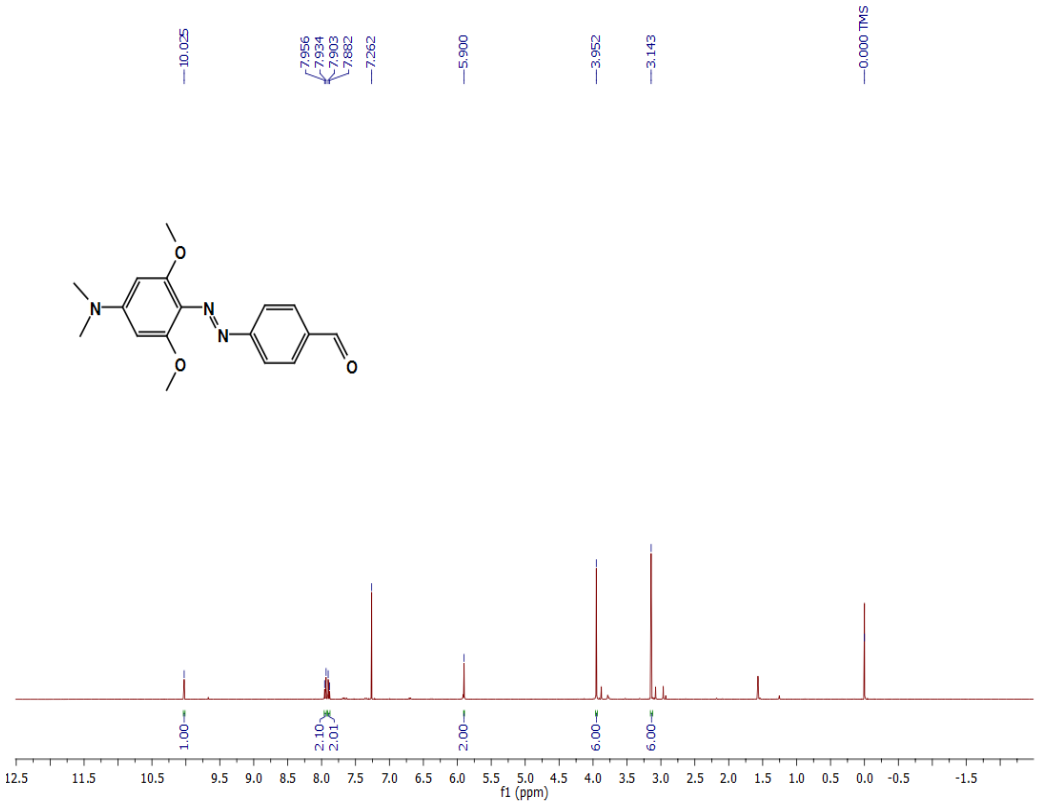

Fig. 3.5 ^{1}H NMR of Az III

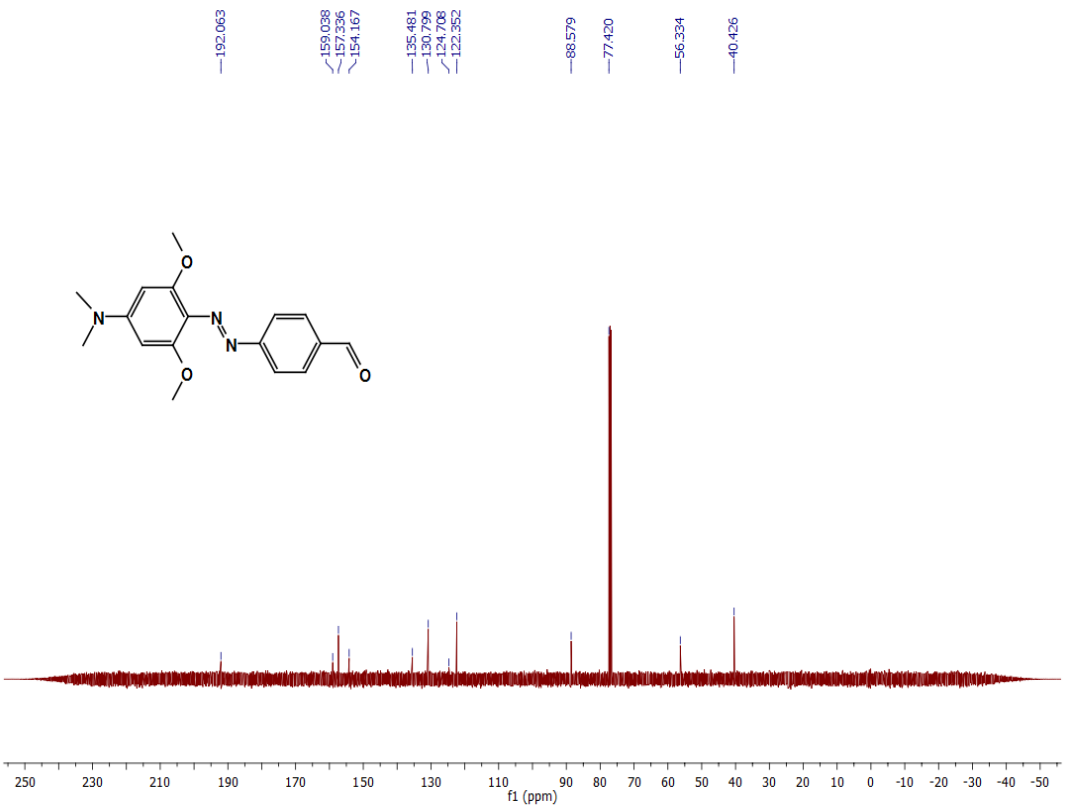

Fig. 3.6 ^{13}C NMR of Az III

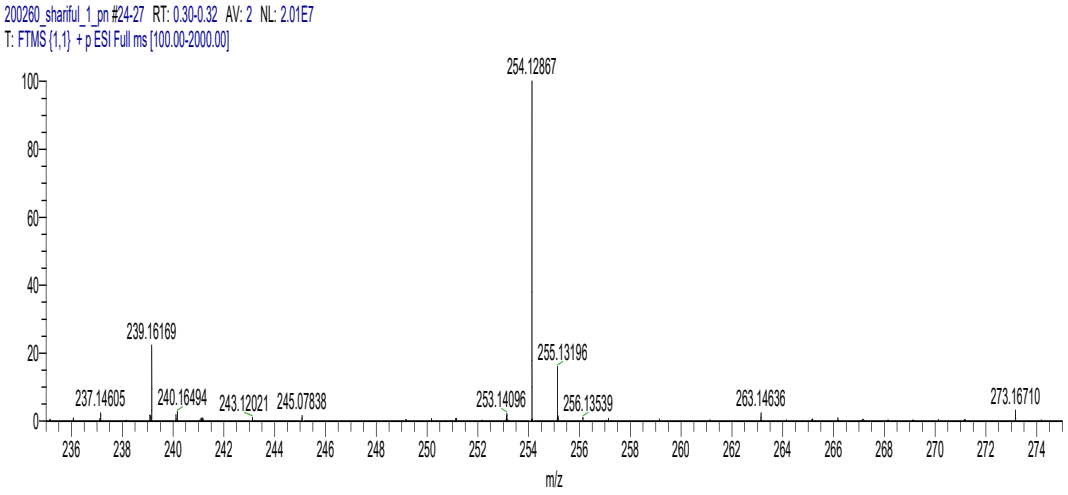

Fig. 3.7 High-resolution mass spectra of Az I. Observed and theoretical MS for $C_{15}H_{16}N_3O$ $[M + H]^+$: 254.12867 and 254.12879.

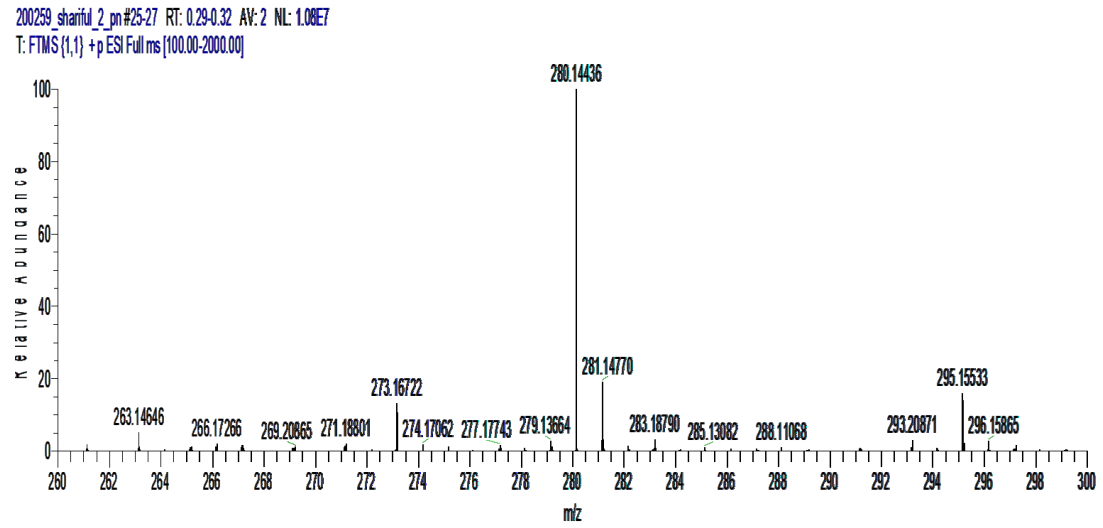

Fig. 3.8 High-resolution mass spectra of Az II. Observed and theoretical MS for $C_{17}H_{18}N_3O$ $[M + H]^+$: 280.14436 and 280.14444.

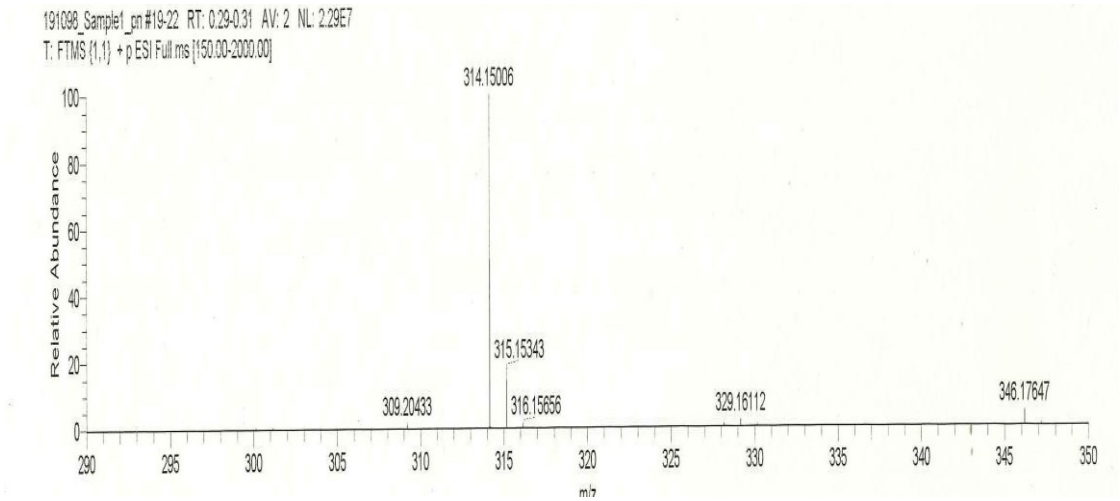

Fig. 3.9 High-resolution mass spectra of Az III. Observed and theoretical MS for $C_{17}H_{18}N_3O$ $[M + H]^+$: 280.15006 and 280.14992.

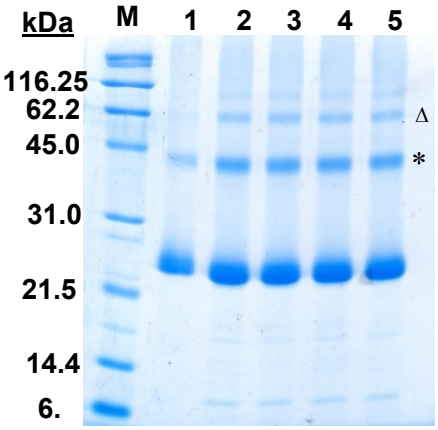

Fig. 3.10 SDS-PAGE analysis of azo chromophore Az I analogues of wild-type POP and POP mutant proteins. Lane M, protein molecular weight maker. Lanes 1-5 gave bands for wild-type PR, PAz I, PAz I-D97N, PAz I-D227N and PAz I-E108Q respectively. *,Δ SDS-PAGE bands might be due to the formation of dimer and trimer of POP.

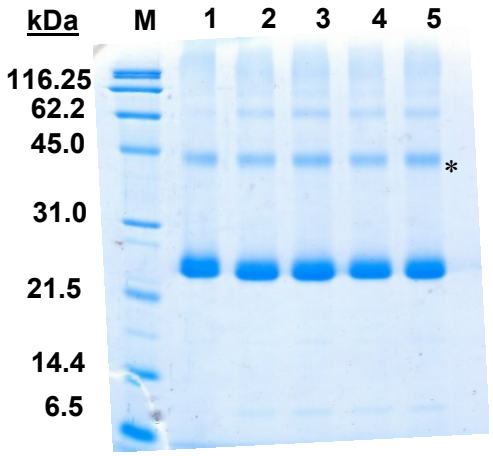

Fig. 3.11 SDS-PAGE analysis of azo chromophore Az II analogues of wild-type POP and POP mutant proteins. Lane M, protein molecular weight maker. Lanes 1-5 gave band for wild-type PR, PAz II, PAz II-D97N, PAz II-D227N and PAz II-E108Q respectively. * SDS-PAGE bands might be due to the formation of dimer of POP.

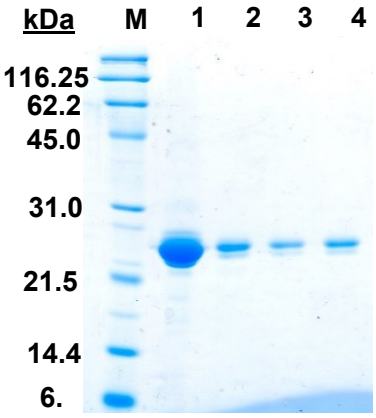

Fig. 3.12 SDS-PAGE analysis of azo analogues of BR. Lane M, protein molecular weight maker. Lanes 1-4 gave bands for wild-type BR, BOP, BAz I and BAz II respectively.

4. Conclusion

In this study, the author has investigated the development, photoinduced proton transfers, and photocycles of azo chromophore–bound POP and BOP. Through mutational studies the author has also demonstrated that the microbial opsin proteins control the chemical stability and photochemical reactions of the azo-bound pigments. Although they undergo photocycling and proton transfer reactions, these azo pigments did not pump protons. In contrast to the wild-type PR and BR, our azo analogues of PR and BR accept the proton initially from the hydrophilic EC side with subsequent proton release to the same side, because their Schiff bases were not protonated in the initial state. Moreover, analysis of flash photolysis data indicated that the thermal isomerization might be too rapid for the protein conformational change to induce deprotonation of the donor residue. An azo chromophore that could form a protonated Schiff base in the initial state and undergo proton release initially upon illumination and, thereby, induce an appropriate conformational change would drive the proton pumping function. In future studies the author will synthesize azo chromophores with electron-donating substituents to bind with microbial opsin proteins through protonated Schiff base units; the lower basicity of the Schiff base upon illumination should then lead to initial proton release and an optimal thermal isomerization rate to induce the required conformational change of the protein. This present study confirms that photoisomerization of azo chromophore units can induce conformational changes of microbial opsin proteins. The author is also interested in studying other aspects of the photofunctional properties of these new azo chromophore–bound POP and BOP.

5. References

1. O. P. Ernst, D. T. Lodowski, M. Elstner, P. Hegemann, L. S. Brown and H. Kandori, *Chem. Rev.*, 2014, **114**, 126–63.
2. J. L. Spudich, C. Yang, K. Jung and E. N. Spudich, *Annu. Rev. Cell Dev. Biol*., 2000, **16**, 365–92.
3. E. G. Govorunova, O. A. Sineshchekov, H. Li and J. L. Spudich, *Annu. Rev. Biochem.*, 2017, **86**, 845–72.
4. K. Inoue, Y. Kato and H. Kandori, *Trends Microbiol*., 2015, **23**, 91–98.
5. O. Beja, L. Aravind, E. V. Koonin, M. T. Suzuki, A. Hadd, L. P. Nguyen, S. B. Jovanovich, C. M. Gates, R. A. Feldman, J. L. Spudich, E. N. Spudich and E. F. DeLong, *Science*, 2000, **289**, 1902–1906.
6. H. Kandori, *Front. Mol. Biosci.*, 2015, **2**, 1–11.
7. M. Dong, A. Babalhavaeji, C. V. Collins, K. Jarrah, O. Sadovski, Q. Dai and G. A. Wolley, *J. Am. Chem. Soc.,* 2017, **139**, 13483–13486.
8. H. M. D. Bandara and S. C. Burdette, *Chem. Soc. Rev*., 2012, **41**, 1809–1825.
9. F. Zhang, K. A. Timm, K. M. Arndt and G. A. Woolley, *Angew. Chemie. – Int. Ed.*, 2010, **49**, 3943–3946.
10. P. Stawski, M. Sumser and D. Trauner, *Angew. Chemie. – Int. Ed.,* 2012, **51**, 5748–5751.
11. K. R. S. Kumar, T. Kamei, T. Fukaminato and N. Tamaoki, *ACS Nano,* 2014, **8**, 4157–4165.
12. A. K. Singh, J. Das and N. Majumdar, *J. Am. Chem. Soc.,* 1996, **118**, 6185–6191.
13. I. Logunov and K. Schulten, *J. Am. Chem. Soc.,* 1996, **118**, 9727–9735.

14. K. Koyama, T. Miyasaka, R. Needleman and J. K. Lanyi, *Photochem. Photobiol.,* 1998, **68,** 400–406.

15. J. Tamogami, T. Kikukawa, S. Miyauchi, E. Muneyuki and N. Kamo, *Photochem. Photobiol.,* 2009, **85**, 578–589.

16. J. Tamogami, T. Kikukawa, T. Nara, K. Shimono, M. Demura and N. Kamo, *Biochemistry*, 2012, **51**, 9290–9301.

17. J. Tamogami, T. Kikukawa, Y. Ikeda, A. Takemura, M. Demura and N. Kamo, *Biophys. J.,* 2010, **98**, 1353–1363.

18. A. K. Dioumaev, L. S. Brown, J. Shih, E. N. Spudich, J. L. Spudich and J. K. Lanyi, *Biochemistry*, 2002, **41**, 5348–5358.

19. T. Friedrich, S. Geibel, R. Kalmbach, I. Chizhov, K. Ataka, J. Heberle, M. Engelhard and E. Bamberg, *J. Mol. Biol*., 2002, **321**, 821–838.

20. G. Varo, L. S. Brown, M. Lakatos and J. K. Lanyi, *Biophys. J*., 2003, **84**, 1202–1207.

21. P. D. Wildes, J. G. Pacifici, G. Irick and D. G. Whitten, *J. Am. Chem. Soc.*, 1971, **93**, 2004–2008.

22. F. Bou-Abdallah, G. Zhao, H. R. Mayne, P. Arosio and N. D. Chasteen, *J. Am. Chem. Soc.,* 2005, **127**, 3885–3893.

23. W. W. Wang, O. A. Sineshchekov, E. N. Spudich and J. L. Spudich, *J. Biol. Chem.*, 2003, **278**, 33985–33991.

24. E. S. Imasheva, S. P. Balashov, J. M. Wang, A. K. Dioumaev and J. K. Lanyi, *Biochemistry*, 2004, **43**, 1648–1655.

25. D. Ikeda, Y. Furutani and H. Kandori, *Biochemistry,* 2007, **46,** 5365–5373.

26. E. S. Imasheva, K. Shimono, S. P. Balashov, J. M. Wang, U. Zadok, M.

Sheves, N. Kamo and J. K. Lanyi, *Biochemistry*, 2005, **44**, 10828–10838.

27. M. Andersson, E. Malmerberg, S. Westenhoff, G. Katona, M. Cammarata, A. B. Wöhri, L. C. Johansson, F. Ewald, M. Eklund, M. Wulff, J. Davidsson and R. Neutze, *Structure,* 2009, **17**, 1265–1275.
28. E. Freier, S. Wolf and K. Gerwert, *Proc. Natl. Acad. Sci. U. S. A*., 2011, **108**, 11435–11439.
29. G. Váró and J. K. Lanyi, *Biophys. J*., 1991, **59**, 313–322.
30. C. Ganea, C. Gergely, K. Ludmann and G. Váró, *Biophys. J.*, 1997, **73**, 2718–2725.
31. L. S. Brown, G. Váró, R. Needleman and J. K. Lanyi, *Biophys. J.,* 1995, **69**, 2103–2111.
32. R. Tunuguntla, M. Bangar, K. Kim, P. Stroeve, C.M. Ajo-Franklin and A. Noy, *Biophys J.,* 2013, **105**, 1388–1396.
33. E. Racker and W. Stoeckenius, *J. Biol. Chem.,* 1974, 249, 662–663.
34. F. Garczarek, L. S. Brown, J. K. Lanyi and K. Gerwert, *Proc. Natl. Acad. Sci. U. S. A.*, 2005, **102**, 3633–3638.
35. F. Garczarek and K. Gerwert, *Nature,* 2006, 439, 109–112.
36. S. Samanta, A. Babalhavaeji, M. Dong and G. A. Woolley, *Angew. Chem. Int. Ed.,* **2013**, 52, 14127-14130.
37. H. Rau, *Angew. Chemie. Int. – Ed.*, 1973, **12**, 224–235.
38. A. P. Lill, C. B. Rödl, D. Steinhilber, H. Stark and B. Hofmann, *Eur. J. Med. Chem*., 2015, 89, 503–523.
39. K. S. Park, Y. Seo, M. K. Kim, K. Kim, Y. K. Kim, H. Choo and Y. Chong, *Org. Biomol. Chem.*, 2015, **13**, 11194–11199.

40. P. M. Javier, Y. Zhao, K. Clays, M. G. Kuzyk, Y. Shen, L. Qiu, J. Hao and K. Guo, *J. Am. Chem. Soc*., 2009, **131,** 5084–5093.

41. D. Oesterhelt, *Methods Enzymol.*, 1974, **31C**, 667–678.

42. D. Oesterhelt and L. Schuhmann, *FEBS Lett.,* 1974, **44**, 262–265.

43. M. J. Pettei, A. P. Yudd, K. Nakanishi, R. Henselman and W. Stoeckenius, *Biochemistry,* 1977, **16**, 1955–1959.

44. M. Iwamoto, K. Shimono, M. Sumi, K. Koyama and N. Kamo, *J. Phys. Chem. B.*, 1999, **103**, 10311–10315.

45. M. Iwamoto, C. Hasegawa, Y. Sudo, K. Shimono, T. Araiso and N. Kamo, *Biochemistry,* 2004, **43**, 3195–3203.

46. M. Sato, T. Kikukawa, T. Araiso, H. Okita, K. Shimono, N. Kamo, M. Demura and K. Nitta, *J Biochem.*, 2003, **134**, 151–158.

List of publication

(1) " Photoisomerization of azobenzene units drives the photochemical reaction cycles of proteorhodopsin and bacteriorhodopsin analogues "

Shariful Haque, Takashi Kikukawa and Nobuyuki Tamaoki, *Org. Biomol. Chem.*, 2020, **18**, 6312

Acknowledgements

The author expresses his sincere gratitude and thank to his supervisor Professor Nobuyuki Tamaoki for his guidance, inspiration, and continuous support throughout the doctoral research.

The author also expresses his heartfelt gratitude and thank to his co-supervisor Dr. Takashi Kikukawa (Hokkaido University) for his valuable guidance, inspiration and continuous support throughout the doctor research.

The author would like to thank Dr. Jun Tamogami (Matsuyama University) for providing us the expression plasmids of PO and the mutants.

The author would like to thank all former and current members of the Professor Tamaoki lab (2017-2020), Dr. Halley M. M., Dr. A., S., Amrutha, Dr. Md. J. Islam, Dr. Ms. N., N., Mafy, Mr. Sampreeth T., Mr. Shakkeeb T., Mr. Ashino F., Mr. T., Muramatsu, Mr. K., Ueda, Mr. K. Yamashita, Mr. Qi Jiajun, Mr. Lin Runze, Mr. S. Yutani, and Mr. G. Mizushima. The author gratefully acknowledges associate professor Dr. Yuna Kim, former assistant professor Dr. Yoshimitsu Sagara, and assistant professor Dr. Kazuya Matsuo in Professor Tamaoki lab for their warm suggestion and support.

The author also wants to thank all the former and present member in Dr. Takashi Kikukawa Lab (2017-2020) for the friendly support during my research work.

The author would like to thank cordially the teachers and students of Department of Pharmacy, Pabna University of Science and Technology, Bangladesh for their support and prayer.

The author acknowledges the program organizers of IGP.

The author was financially supported by Japan Government (MEXT scholarship) and Bangladesh Government.

Finally, the author greatly appreciates and thank his all family members (particularly, my mother, parents in law, wife, son, daughter, sisters, brothers in law, nephews, niece) and other relatives for their absolutely and timely essential support. The author thanks all his friends in Japan and Bangladesh for helpful and hearty support.